System analysis of a Diesel Engine with VGT and EGR

Johan Wahlström, Lars Eriksson, and Lars Nielsen

Vehicular systems
Department of Electrical Engineering
Linköpings universitet, SE-581 83 Linköping, Sweden
WWW: www.vehicular.isy.liu.se
E-mail: {johwa, larer, lars}@isy.liu.se
Report: LiTH-ISY-R-2881

March 16, 2009

Abstract

A system analysis of a diesel engine with VGT and EGR is performed in order to obtain insight into a VGT and EGR control problem where the goal is to control the performance variables oxygen fuel ratio λ_O and EGR-fraction x_{egr} using the VGT actuator u_{vgt} and the EGR actuator u_{egr}. Step responses over the entire operating region show that the channels $u_{vgt} \rightarrow \lambda_O$, $u_{egr} \rightarrow \lambda_O$, and $u_{vgt} \rightarrow x_{egr}$ have non-minimum phase behaviors and sign reversals. The fundamental physical explanation of these system properties is that the system consists of two dynamic effects that interact: a fast pressure dynamics in the manifolds and a slow turbocharger dynamics. It is shown that the engine frequently operates in operating points where the non-minimum phase behaviors and sign reversals occur for the channels $u_{vgt} \rightarrow \lambda_O$ and $u_{vgt} \rightarrow x_{egr}$, and consequently, it is important to consider these properties in a control design. Further, an analysis of zeros for linearized multiple input multiple output models of the engine shows that they are non-minimum phase over the complete operating region. A mapping of the performance variables λ_O and x_{egr} and the relative gain array show that the system from u_{egr} and u_{vgt} to λ_O and x_{egr} is strongly coupled in a large operating region. It is also illustrated that the pumping losses $p_{em} - p_{im}$ decrease with increasing EGR-valve and VGT opening for almost the complete operating region.

Contents

1 Introduction **1**

2 Diesel engine model **1**

3 Physical intuition for system properties **2**
3.1 Physical intuition for VGT position response 3
3.2 Physical intuition for EGR-valve response 3

4 Mapping of system properties **5**
4.1 DC-gains 6
4.2 Zeros and a root locus 12
4.3 Non-minimum phase behaviors 15
4.4 Operation pattern for the European Transient Cycle 19
4.5 Response time 19

5 Mapping of performance variables **21**
5.1 System coupling in steady state 21
5.2 Pumping losses in steady state 21

6 Conclusions **24**

A Response time **26**

B Relative gain array **31**

1 Introduction

Legislated emission limits for heavy duty trucks are constantly reduced. To fulfill the requirements, technologies like Exhaust Gas Recirculation (EGR) systems and Variable Geometry Turbochargers (VGT) have been introduced. The primary emission reduction mechanisms utilized to control the emissions are that NO_x can be reduced by increasing the intake manifold EGR-fraction x_{egr} and smoke can be reduced by increasing the oxygen/fuel ratio λ_O [1]. Therefore, it is natural to choose x_{egr} and λ_O as the main performance variables. However x_{egr} and λ_O depend in complicated ways on the EGR and VGT actuation, and it is therefore necessary to have coordinated control of the EGR and VGT to reach the legislated emission limits in NO_x and smoke. When developing a controller for this system, it is desirable to perform an analysis of the characteristics and the behavior of the system in order to obtain insight into the control problem. This is known to be important for a successful design of an EGR and VGT controller due to non-trivial intrinsic properties, see for example [3]. Therefore, the goal is to make a system analysis of the diesel engine model in Sec. 2. The essential system properties for this model are physically explained in Sec. 3 by looking at step responses. In Sec. 4 a mapping of these system properties is performed by simulating step responses over the entire operating region and by analyzing zeros for linearized models. This is done for the main performance variables oxygen/fuel ratio, λ_O, and EGR-fraction, x_{egr}. Further, λ_O and x_{egr} are mapped in Sec. 5 in order to investigate the interactions in the system. Also, the pumping work is mapped in Sec. 5 to give insight into how the pumping losses can be minimized.

2 Diesel engine model

A model for a heavy duty diesel engine is used in the system analysis in this report. This diesel engine model is focused on the gas flows, see Fig. 1, and it is a mean value model with eight states: intake and exhaust manifold pressures (p_{im} and p_{em}), oxygen mass fraction in the intake and exhaust manifold (X_{Oim} and X_{Oem}), turbocharger speed (ω_t), and three states describing the actuator dynamics for the two control signals ($\tilde{u}_{egr1}$, $\tilde{u}_{egr2}$, and $\tilde{u}_{vgt}$). These states are collected in a state vector x

$$x = [p_{im} \quad p_{em} \quad X_{Oim} \quad X_{Oem} \quad \omega_t \quad \tilde{u}_{egr1} \quad \tilde{u}_{egr2} \quad \tilde{u}_{vgt}]^T$$

There are no state equations for the manifold temperatures, since the pressures and the turbocharger speed govern the most important system properties, such as non-minimum phase behaviors, overshoots, and sign reversals, while the temperature states have only minor effects on these system properties [7].

The resulting model is expressed in state space form as

$$\dot{x} = f(x, u, n_e)$$

where the engine speed n_e is considered as an input to the model, and u is the control input vector

$$u = [u_\delta \quad u_{egr} \quad u_{vgt}]^T$$

which contains mass of injected fuel u_δ, EGR-valve position u_{egr}, and VGT actuator position u_{vgt}.

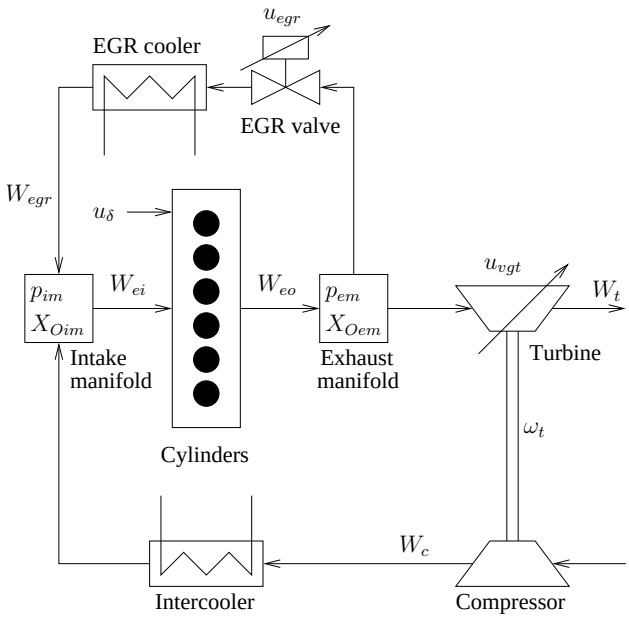

Figure 1: Sketch of the diesel engine model used for the system analysis. It has five states related to the engine (p_{im}, p_{em}, X_{Oim}, X_{Oem}, and ω_t) and three for actuator dynamics ($\tilde{u}_{egr1}$, $\tilde{u}_{egr2}$, and $\tilde{u}_{vgt}$).

A detailed description and derivation of the model together with a model tuning and a validation against test cell measurements is given in [7]. The validation shows that the model captures the essential system properties that exist in the diesel engine, i.e. non-minimum phase behaviors, overshoots, and sign reversals. The references [3], [2], and [4] also show that the diesel engine has these system properties.

3 Physical intuition for system properties

As mentioned in Sec. 2, the diesel engine has non-minimum phase behaviors, overshoots, and sign reversals. The fundamental physical explanation of these system properties is that the system consists of two dynamic effects that interact: a fast pressure dynamics in the manifolds and a slow turbocharger dynamics. These two dynamic effects often work against each other which results in the system properties above. For example, if the fast dynamic effect is small and the slow dynamic effect is large, the result will be a non-minimum phase behavior, see λ_O in Fig. 2. Note that the DC-gain is negative. However, if the fast dynamic effect is large and the slow dynamic effect is small, the result will be an overshoot and a sign reversal, see λ_O in Fig. 3. The precise conditions for this sign reversal are due to complex interactions between flows, temperatures, and pressures in the entire engine. More physical explanations of the system properties for VGT position and EGR-valve responses are found in the following sections.

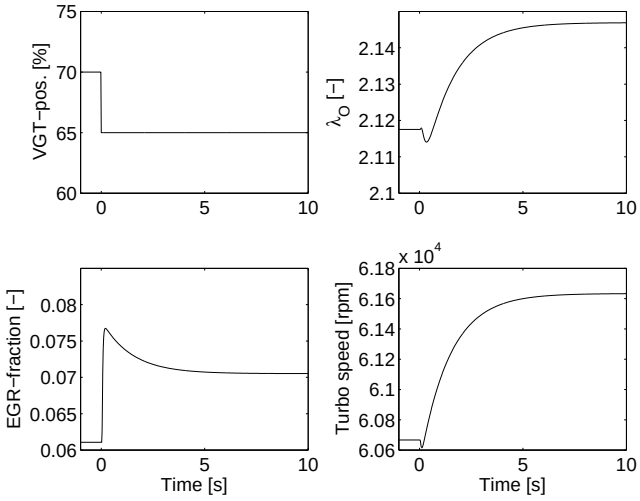

Figure 2: Responses to a step in VGT position showing non-minimum phase behaviors in λ_O and in the turbo speed. Operating point: u_δ=110 mg/cycle, n_e=1500 rpm and u_{egr}=80 %. Initial u_{vgt}=70 %.

3.1 Physical intuition for VGT position response

Model responses to steps in VGT position are shown in Fig. 2 and 3. In Fig. 2 a closing of the VGT leads to an increase in exhaust manifold pressure and therefore an increase in EGR-fraction which leads to a decrease in intake manifold oxygen mass fraction and a decrease in λ_O in the beginning of the step. However, an increase in exhaust manifold pressure thereafter leads to an increase in turbocharger speed and thus compressor mass flow. The result is an increase in λ_O and in this case the increase is larger than the initial decrease. The increase in λ_O is slower due to the slower dynamics of the turbocharger speed, which means that VGT position to λ_O has a non-minimum phase behavior. There is also a non-minimum phase behavior in the turbocharger speed response. The non-minimum phase behavior in λ_O increases with increasing EGR-valve opening and decreasing VGT opening until the sign of the DC-gain is reversed and the non-minimum phase behavior becomes an overshoot instead. The sign reversal can be seen in Fig. 3, where the size of the step is the same but the initial VGT position is more closed compared to Fig. 2. Contrary to Fig. 2, Fig. 3 shows that a closing of the VGT position leads to a total decrease in λ_O. Further, the non-minimum phase behavior in the turbocharger speed response in Fig. 3 is larger than in Fig. 2.

3.2 Physical intuition for EGR-valve response

Model responses to steps in the EGR-valve are shown in Fig. 4 and 5. In Fig. 4, λ_O has a non-minimum phase behavior which has the following physical explanation. The closing of the EGR-valve leads to an immediate decrease in EGR-fraction, yielding an immediate decrease in p_{im} and increase in p_{em}. However, closing the EGR-valve also means that less exhaust gases are recirculated and there are thus more exhaust gases to drive the turbine. This causes the

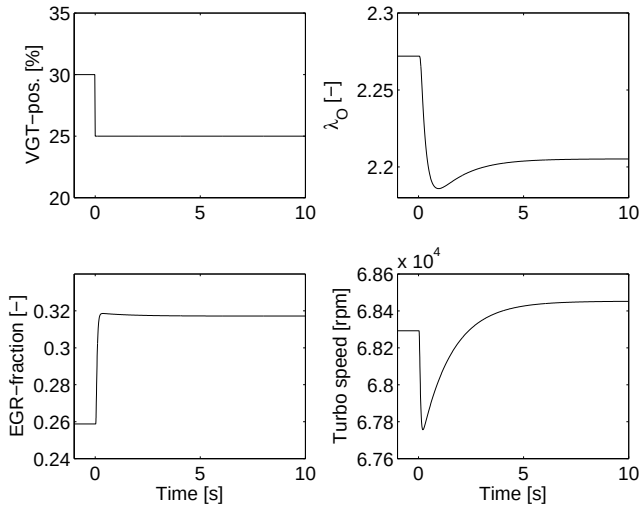

Figure 3: Responses to a step in VGT position showing a sign reversal in λ_O compared to Fig. 2. Operating point: u_δ=110 mg/cycle, n_e=1500 rpm and u_{egr}=80 %. Initial u_{vgt}=30 %.

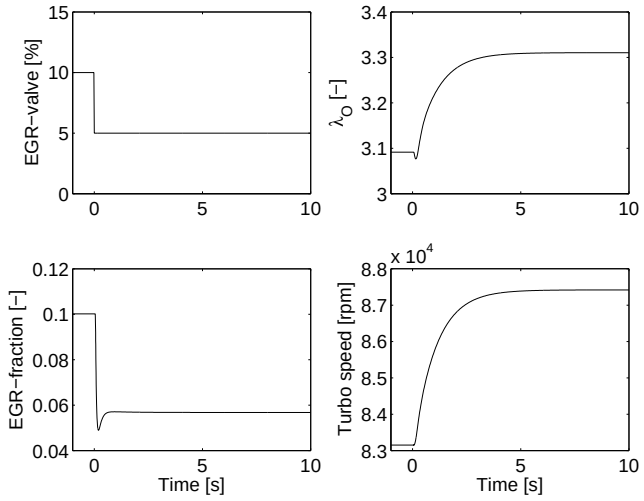

Figure 4: Responses to a step in EGR-valve showing a non-minimum phase behavior in λ_O. Operating point: u_δ=110 mg/cycle, n_e=1500 rpm and u_{vgt}=30 %.

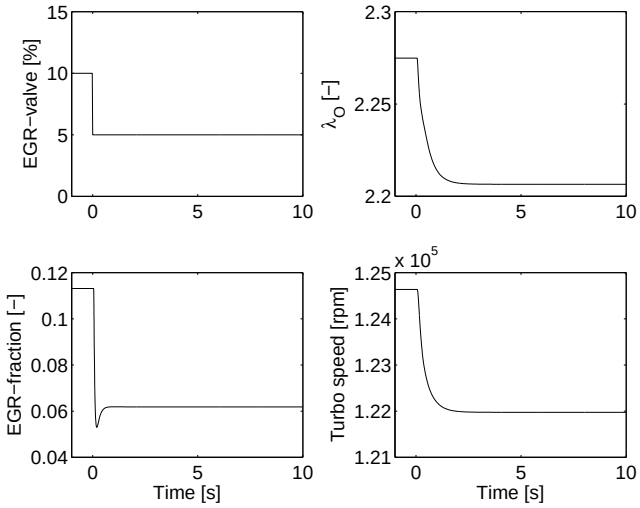

Figure 5: Responses to a step in EGR-valve showing sign reversals in λ_O and in the turbo speed compared to Fig. 4. Operating point: u_δ=230 mg/cycle, n_e=2000 rpm and u_{vgt}=30 %.

turbocharger to speed up and produce more compressor flow which results in a subsequent increase in p_{im} that is larger than the initial decrease. This effect is slower though due to the slower dynamics of the turbocharger speed, which gives that EGR-valve to p_{im} has a non-minimum phase behavior. Since p_{im} affects the total flow into the engine and thereby λ_O, there is also a non-minimum phase behavior in λ_O. Note that the DC-gain from EGR-valve to λ_O is negative in Fig. 4. The non-minimum phase behavior increases with decreasing EGR-valve opening and increasing engine speed until the sign of the DC-gain is reversed. The sign reversal can be seen in Fig. 5, where the step in EGR-valve is performed in an operating point with higher torque and higher engine speed compared to Fig. 4. In contrast to Fig. 4, Fig. 5 shows that a closing of the EGR-valve leads to a total decrease in λ_O and in n_t.

4 Mapping of system properties

The step responses in Sec. 3 show that there are non-minimum phase behaviors and sign reversals in the main performance variables λ_O and x_{egr}. Knowledge about these system properties and response times in the entire operating region is important when developing a control structure. Therefore, the DC-gain K, the non-minimum phase behavior with an relative undershoot x_N, and the response time τ are mapped by simulating step responses in the entire operating region. The DC-gain K is defined as

$$K = \frac{y_2 - y_0}{\Delta u} \tag{1}$$

where y_0 is the initial value and y_2 is the final value of a step response according to Fig. 6 where the input has a step size Δu. The relative undershoot x_N is

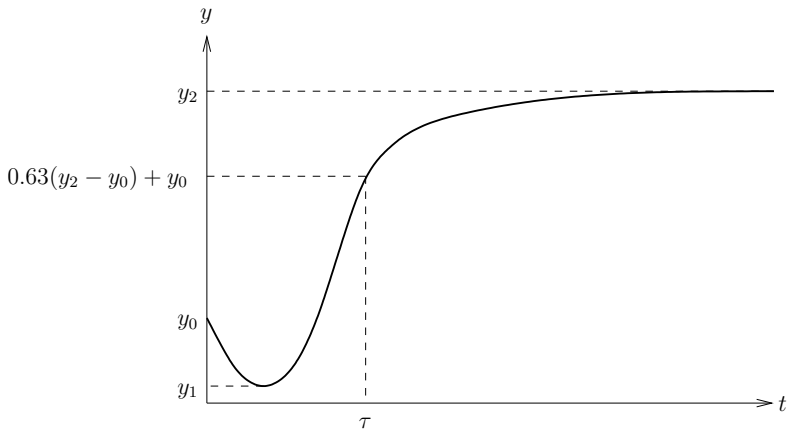

Figure 6: A step response with an initial value y_0, a final value y_2, a non-minimum phase behavior with an undershoot y_1, and a response time τ.

defined as

$$x_N = \frac{y_0 - y_1}{y_2 - y_1} \tag{2}$$

where y_1 is the minimum value of the step response in Fig. 6. The response time τ is defined in Fig. 6, i.e

$$\tau = \{t : y(t) = 0.63(y_2 - y_0) + y_0\} \tag{3}$$

For a first order system with time delay, the response time according to this definition would be the sum of the time constant and the time delay.

The mapping of the system properties is based on step responses simulated at 20 different u_{vgt} points, 20 different u_{egr} points, 3 different n_e points, and 3 different u_δ points. The sizes of the steps in u_{vgt} and u_{egr} are 5% of the difference between two adjoining operating points. Sec. 4.1 presents the results regarding the DC-gains (1). Non-minimum phase zeros for linearized multiple input multiple output (MIMO) models of the engine are analyzed in Sec. 4.2 in order to determine the non-minimum-phase characteristics of these models. A root locus for one operating point is presented in Sec. 4.2 in order to illustrate the poles for the closed loop system. Non-minimum phase behaviors with the relative undershoots (2) are mapped in Sec. 4.3. In addition to a mapping of the system properties over the operating region for the engine, a mapping of the operating points where the engine frequently operates is performed in Sec. 4.4. This is performed by simulating the European Transient Cycle and calculating the relative frequency for different sub-regions. Finally, the response times (3) are mapped in Sec. 4.5.

4.1 DC-gains

A sign reversal in a channel causes problems when controlling the corresponding feedback loop. These sign reversals are investigated by mapping the DC-gain, K, for the channels $u_{vgt} \rightarrow \lambda_O$, $u_{egr} \rightarrow \lambda_O$, $u_{vgt} \rightarrow x_{egr}$, and $u_{egr} \rightarrow x_{egr}$ in Fig. 7 to 10. The channels $u_{vgt} \rightarrow \lambda_O$, $u_{egr} \rightarrow \lambda_O$, and $u_{vgt} \rightarrow x_{egr}$ have

negative DC-gain in large operating regions and reversed sign (positive sign) in small operating regions, while $u_{egr} \rightarrow x_{egr}$ has positive DC-gain in the entire operating region.

The DC-gain for the channel $u_{vgt} \rightarrow \lambda_O$ (see Fig. 7) has reversed sign (positive sign) in operating points with closed to half open VGT, half to fully open EGR-valve, low to medium n_e, and medium to large u_δ or in operating points with half to fully open VGT, low n_e, and small u_δ. The left bottom plot shows that for almost all EGR-valve positions the sign is reversed twice when the VGT goes from closed to fully open. Further, the DC-gain for the channel $u_{egr} \rightarrow \lambda_O$ (see Fig. 8) has reversed sign (positive sign) in a smaller operating region, compared to $u_{vgt} \rightarrow \lambda_O$, which is in operating points with closed to half open EGR-valve, high n_e, and medium to large u_δ. Finally, the DC-gain for the channel $u_{vgt} \rightarrow x_{egr}$ (see Fig. 9) also has reversed sign (positive sign) in a smaller operating region, compared to $u_{vgt} \rightarrow \lambda_O$, which is in operating points with half to fully open VGT, half to fully open EGR-valve, low to medium n_e, and small u_δ.

The DC-gains for all four channels (Fig. 7 to 10) are equal to zero also in some other operating points than where sign reversal occurs. The DC-gains for the channels $u_{egr} \rightarrow \lambda_O$, $u_{vgt} \rightarrow x_{egr}$, and $u_{egr} \rightarrow x_{egr}$ are equal to zero in operating points with half to fully open VGT, low to medium n_e and medium to large u_δ. In these operating points $p_{em} < p_{im}$ (see Fig. 18) which leads to that $x_{egr} = 0$ since no backflow is modeled in the EGR-flow model. As a consequence, the control signal u_{egr} cannot influence the system and the control signal u_{vgt} cannot influence the EGR-fraction. The DC-gain for the channels $u_{egr} \rightarrow \lambda_O$ and $u_{egr} \rightarrow x_{egr}$ are also equal to zero when $u_{egr} = 80$ % and the DC-gain for the channel $u_{vgt} \rightarrow x_{egr}$ is also equal to zero when $u_{egr} = 0$ %.

The mapping of the DC-gains shows that the DC-gains vary much between different operating points in all four channels. A common trend is that the DC-gains for the channels $u_{vgt} \rightarrow \lambda_O$ and $u_{vgt} \rightarrow x_{egr}$ are large when the VGT is closed and small when the VGT is open. Similarly, the DC-gains for the channels $u_{egr} \rightarrow \lambda_O$ and $u_{egr} \rightarrow x_{egr}$ are large when the EGR-valve is closed and small when the EGR-valve is open.

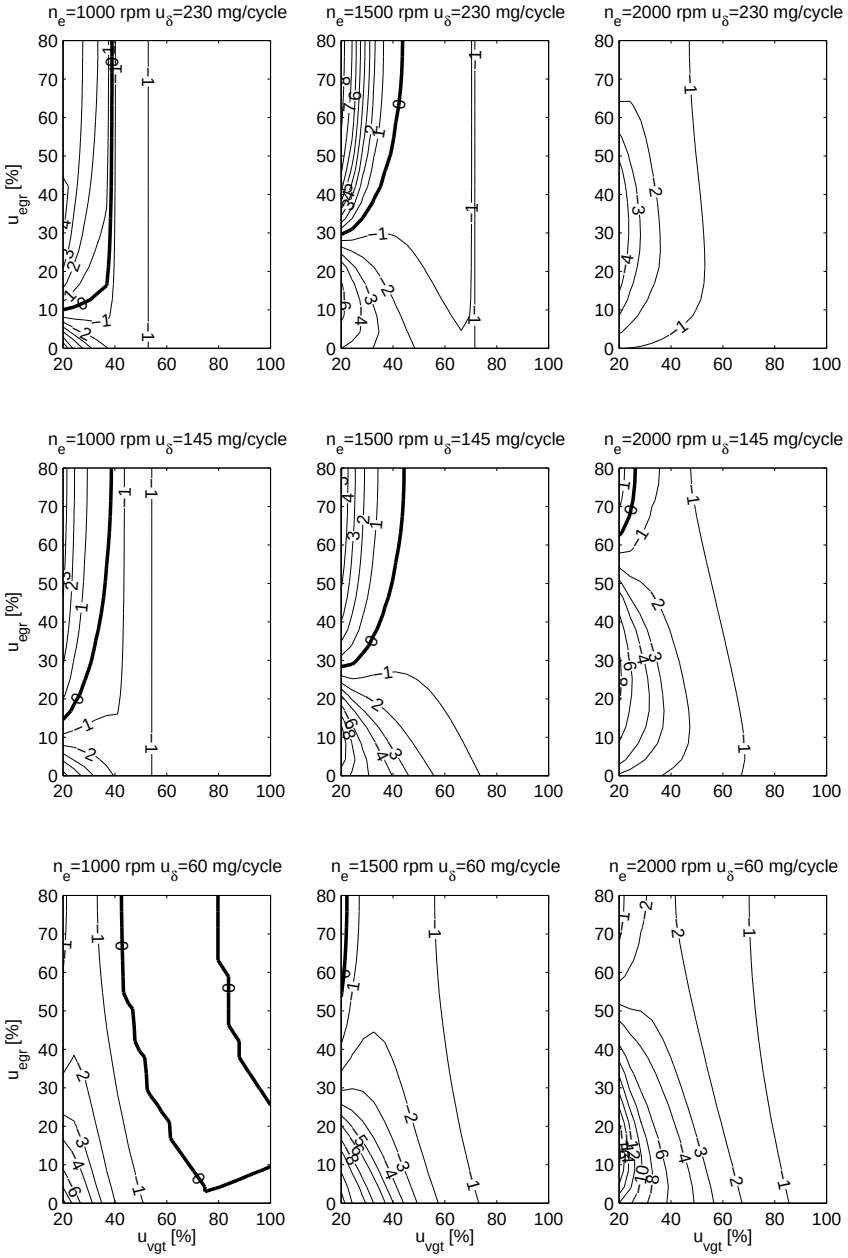

Figure 7: Contour plots of the DC-gain, $100 \cdot K$, for the channel $u_{vgt} \rightarrow \lambda_O$ at 3 different n_e and 3 different u_δ. The DC-gain has a sign reversal that occurs at the thick line.

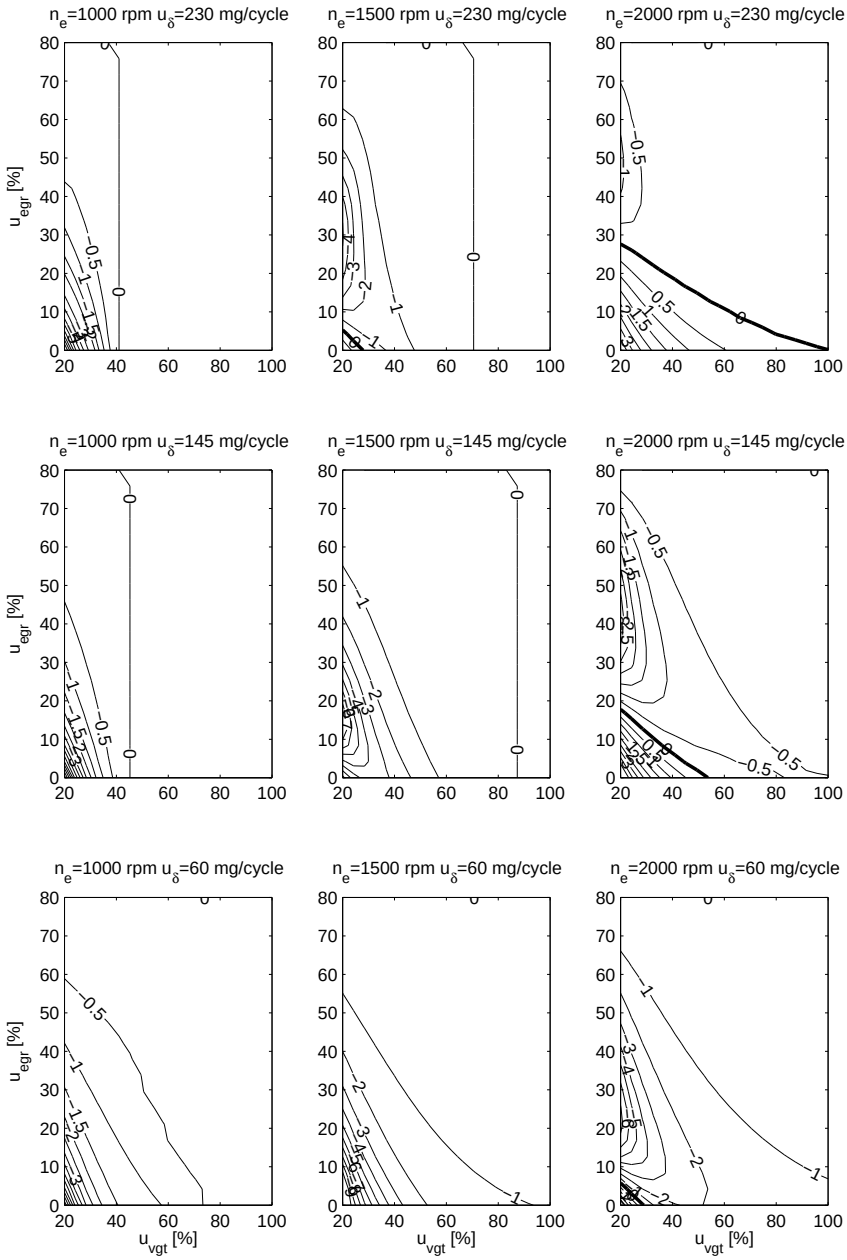

Figure 8: Contour plots of the DC-gain, $100 \cdot K$, for the channel $u_{egr} \rightarrow \lambda_O$ at 3 different n_e and 3 different u_δ. The DC-gain has a sign reversal that occurs at the thick line.

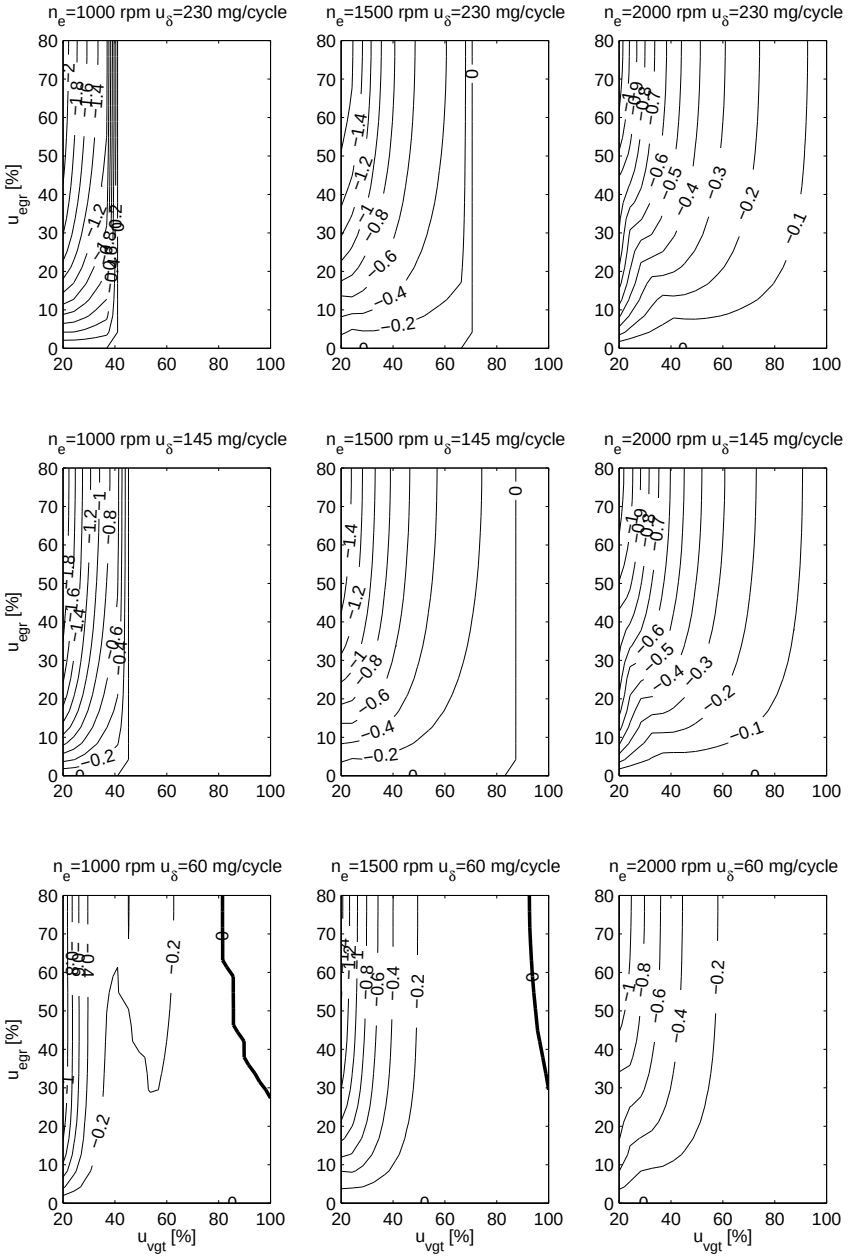

Figure 9: Contour plots of the DC-gain, $100 \cdot K$, for the channel $u_{vgt} \rightarrow x_{egr}$ at 3 different n_e and 3 different u_δ. The DC-gain has a sign reversal that occurs at the thick line.

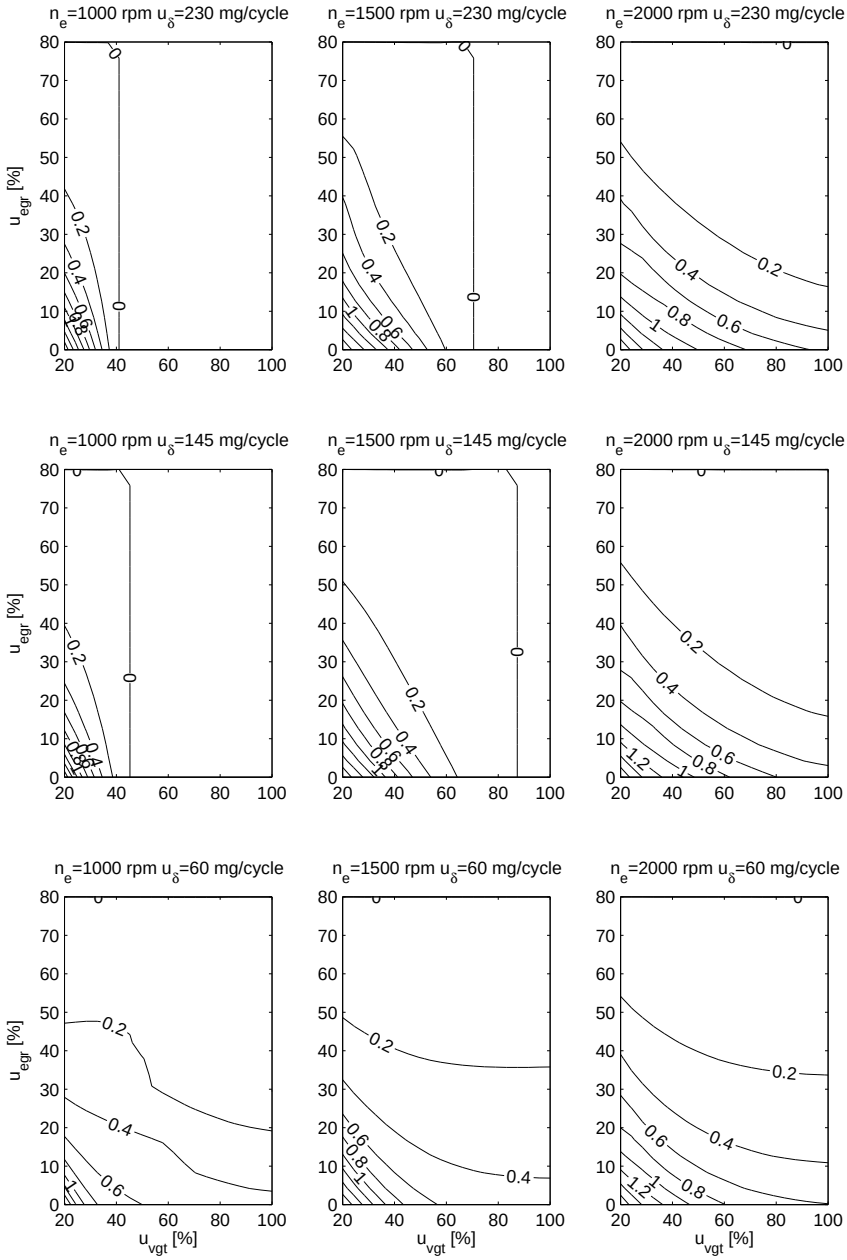

Figure 10: Contour plots of the DC-gain, $100 \cdot K$, for the channel $u_{egr} \rightarrow x_{egr}$ at 3 different n_e and 3 different u_δ. The DC-gain is positive and also equal to zero in some operating points.

4.2 Zeros and a root locus

A mapping of zeros for linearized MIMO models of the engine over the entire operating region is performed in order to determine the non-minimum-phase characteristics of these models. The linear models are constructed by linearizing the non-linear model in Sec. 2 in the same operating points as the operating points in Fig. 7 to 10, i.e. 20 different u_{vgt} points, 20 different u_{egr} points, 3 different n_e points, and 3 different u_δ points. The linear models have the form

$$\begin{aligned} \dot{x} &= A_i\, x + B_i\, u \\ y &= C_i\, x \end{aligned} \tag{4}$$

where i is the operating point number and

$$\begin{aligned} u &= [u_{egr} \quad u_{vgt}]^T \\ x &= [p_{im} \quad p_{em} \quad X_{Oim} \quad X_{Oem} \quad \omega_t \quad \tilde{u}_{egr1} \quad \tilde{u}_{egr2} \quad \tilde{u}_{vgt}]^T \\ y &= [\lambda_O \quad x_{egr}]^T \end{aligned}$$

An analysis of the poles and zeros for the models (4) shows that there are 8 poles in the left complex half plane for the complete operating region, one zero in the right complex half plane for the complete operating region, 3 zeros in the left complex half plane when $p_{em} > p_{im}$, and 2 zeros in the left complex half plane when $p_{em} < p_{im}$. In this latter case the EGR-valve is closed. The value of the zero in the right complex half plane is mapped in Fig. 11 showing that this zero is positive for the complete operating region. Consequently, the linear diesel engine models (4) are non-minimum phase in the complete operating region.

A root locus for the model (4) in one operating point where $p_{em} > p_{im}$ is presented in Fig. 12. This root locus is based on the feedback

$$u = k \begin{pmatrix} \frac{1}{K_{u_{egr}\to\lambda_O}} & 0 \\ 0 & \frac{1}{K_{u_{vgt}\to x_{egr}}} \end{pmatrix} (r - y) \tag{5}$$

where the signal r is the set-point for the output y and the choice of feedback loops is motivated in [5]. The constants $K_{u_{egr}\to\lambda_O}$ and $K_{u_{vgt}\to x_{egr}}$ are the DC-gains for the channels $u_{egr} \to \lambda_O$ and $u_{vgt} \to x_{egr}$ in the operating point $n_e = 1500$ rpm, $u_\delta = 145$ mg/cycle, $u_{egr} = 16.8$ %, and $u_{vgt} = 36.8$ %, and k is a scalar parameter. The root locus in Fig. 12 shows the closed-loop pole trajectories as function of the parameter k. These trajectories have 4 asymptotes due to that the difference between the number of poles and the number of zeros for the open-loop system is 4. Two closed-loop poles become unstable for large k and two poles in the left complex half plane have large imaginary parts for large k, i.e. these poles gives oscillations with low damping. Root loci for other operating points (where $p_{em} > p_{im}$) have approximately the same behavior. Root loci for operating points where $p_{em} < p_{im}$ are not investigated since $x_{egr} = 0$ in these operating points and u_{egr} can not influence the system which leads to that other control modes have to be used in these operating points.

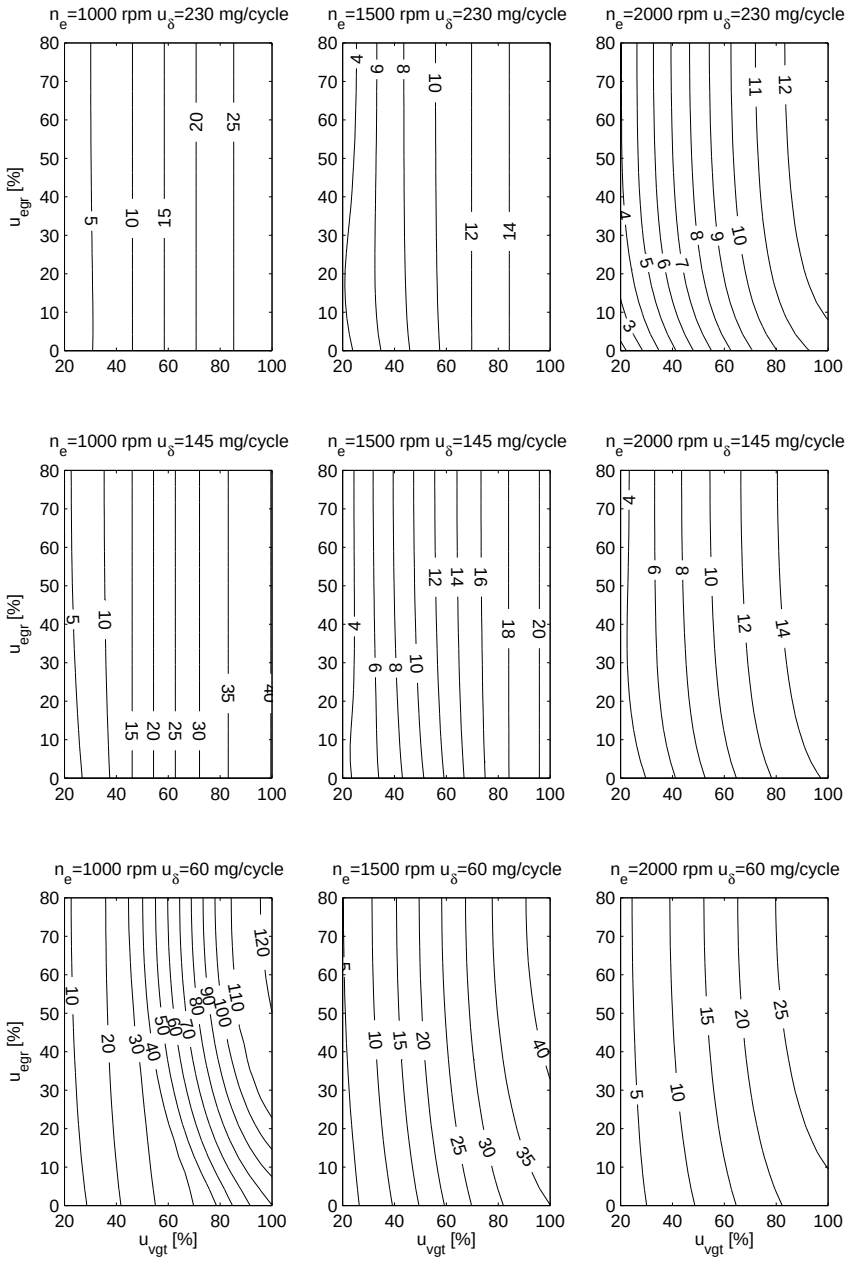

Figure 11: Contour plots of the zero that exists in the right complex half plane showing that this zero is positive for the complete operating region.

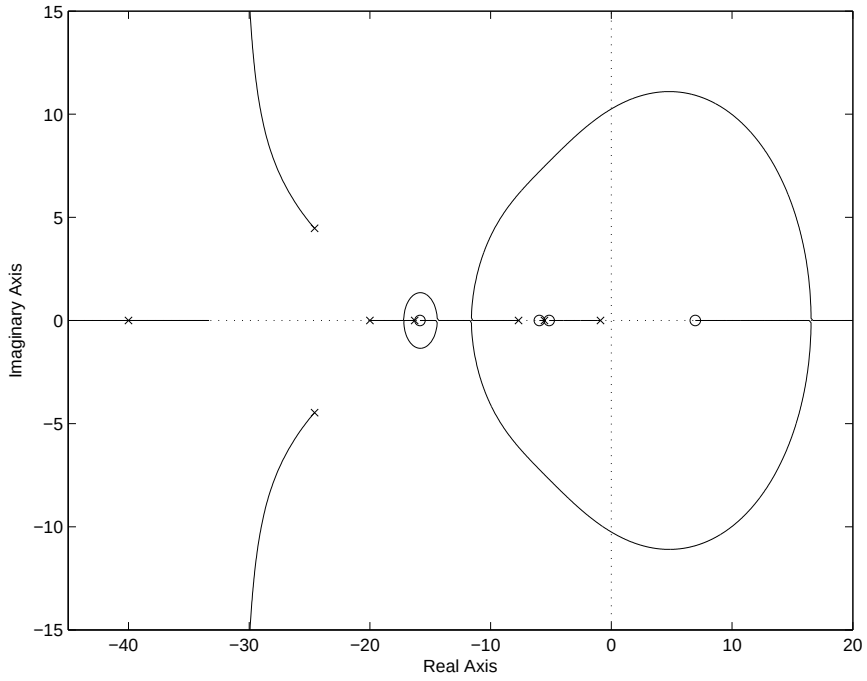

Figure 12: A pole-zero map and a root locus for the model (4) in the operating point $n_e = 1500$ rpm, $u_\delta = 145$ mg/cycle, $u_{egr} = 16.8$ %, and $u_{vgt} = 36.8$ %. The crosses are the poles and the circles are the zeros for the model (4). The root locus shows the closed-loop pole trajectories as function of the scalar parameter k in the feedback (5). The trajectories start at the crosses (poles) with $k = 0$ and ends at the circles (zeros) or along 4 asymptotes with $k = +\infty$.

4.3 Non-minimum phase behaviors

In the previous section, it is shown that the linearized MIMO diesel engine models (4) have a zero in the right half plane and are therefore non-minimum phase. In this section, the size of the undershoot in a non-minimum phase behavior is investigated by mapping the relative undershoot x_N, defined by (2), over the entire operating region. This is performed for the channels $u_{vgt} \rightarrow \lambda_O$, $u_{egr} \rightarrow \lambda_O$, and $u_{vgt} \rightarrow x_{egr}$ in Fig. 13 to 15, but not for the channel $u_{egr} \rightarrow x_{egr}$ as it has no non-minimum phase behavior.

By comparing Fig. 7 with Fig. 13 and comparing Fig. 8 with Fig. 14 it can be seen that the non-minimum phase behaviors in the channels $u_{vgt} \rightarrow \lambda_O$ and $u_{egr} \rightarrow \lambda_O$ only occur in operating points with negative DC-gain. Further, the relative undershoots are 40 to 100 % only in operating points near the sign reversal for these two channels. Consequently, the relative undershoot for the channel $u_{egr} \rightarrow \lambda_O$ is larger than 40 % in a smaller operating region compared to $u_{vgt} \rightarrow \lambda_O$ since the sign reversal for $u_{egr} \rightarrow \lambda_O$ occurs in a smaller operating region. In the operating points with reversed sign (positive sign) the non-minimum phase behavior becomes an overshoot instead (see also Fig. 2 and Fig. 3 where the non-minimum phase behavior in λ_O becomes an overshoot).

By comparing Fig. 9 with Fig. 15 it can be seen that the non-minimum phase behavior in $u_{vgt} \rightarrow x_{egr}$ occurs only in a small operating region with reversed sign (positive sign) for the DC-gain where the relative undershoots are 40 to 100 %. In the operating points with negative DC-gain the non-minimum phase behavior becomes an overshoot instead.

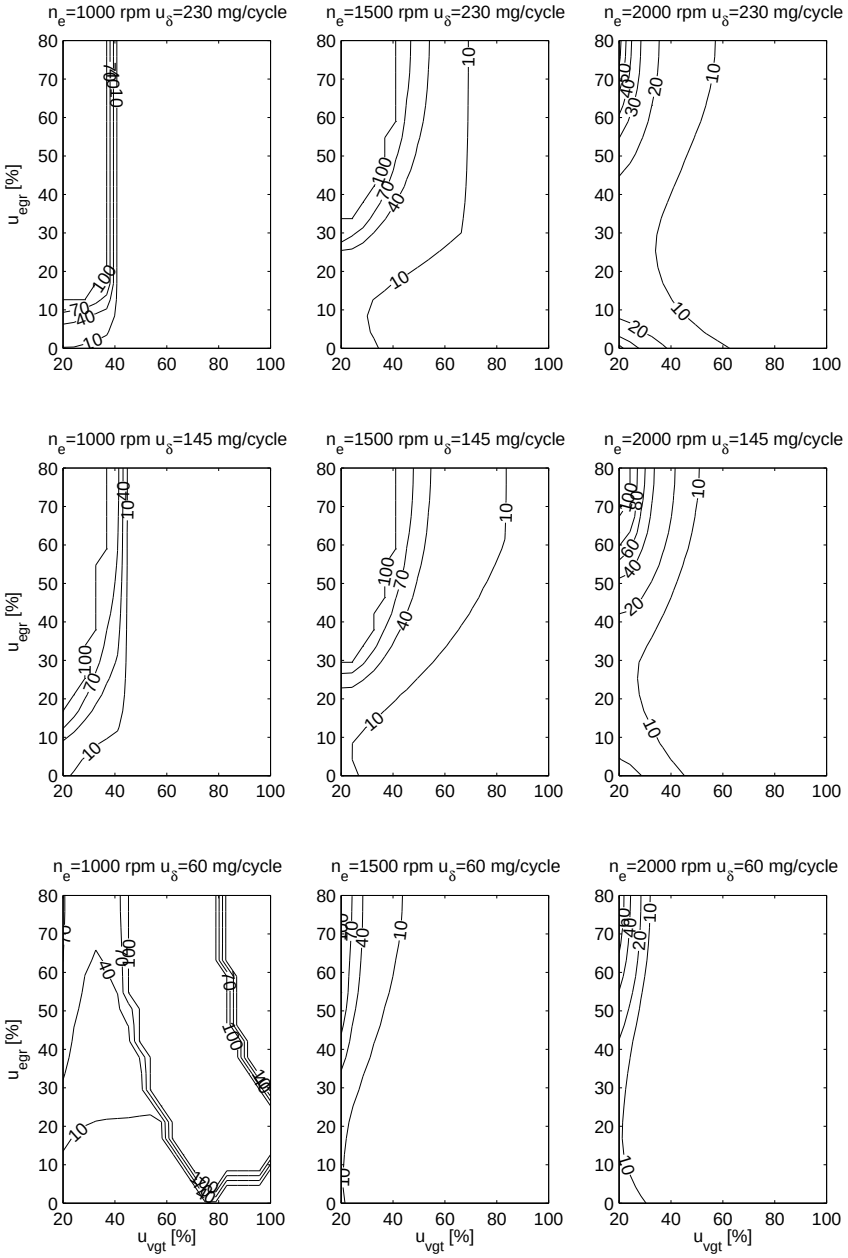

Figure 13: Contour plots of the relative undershoot, $x_N\,[\%]$, (see Eq. (2)) in a non-minimum phase behavior for the channel $u_{vgt} \rightarrow \lambda_O$ at 3 different n_e and 3 different u_δ.

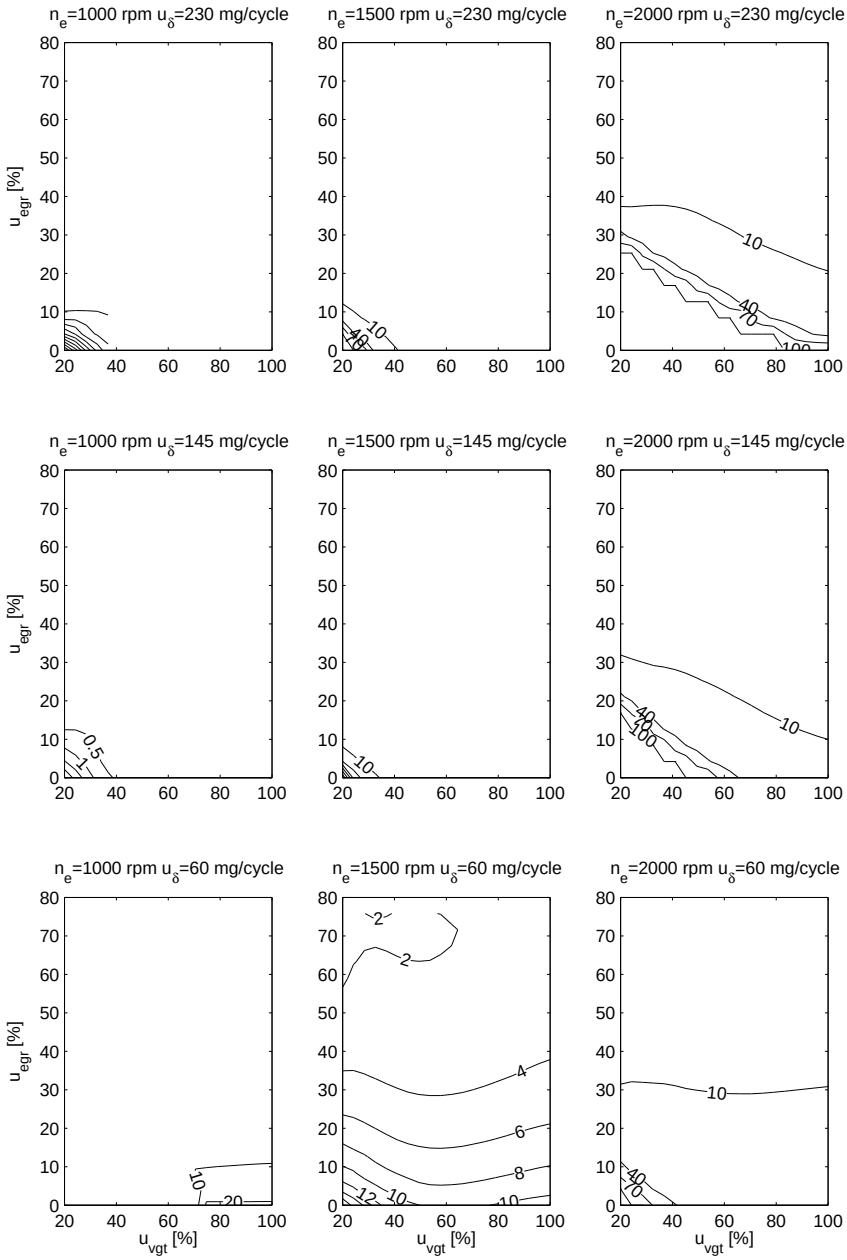

Figure 14: Contour plots of the relative undershoot, x_N [%], (see Eq. (2)) in a non-minimum phase behavior for the channel $u_{egr} \rightarrow \lambda_O$ at 3 different n_e and 3 different u_δ.

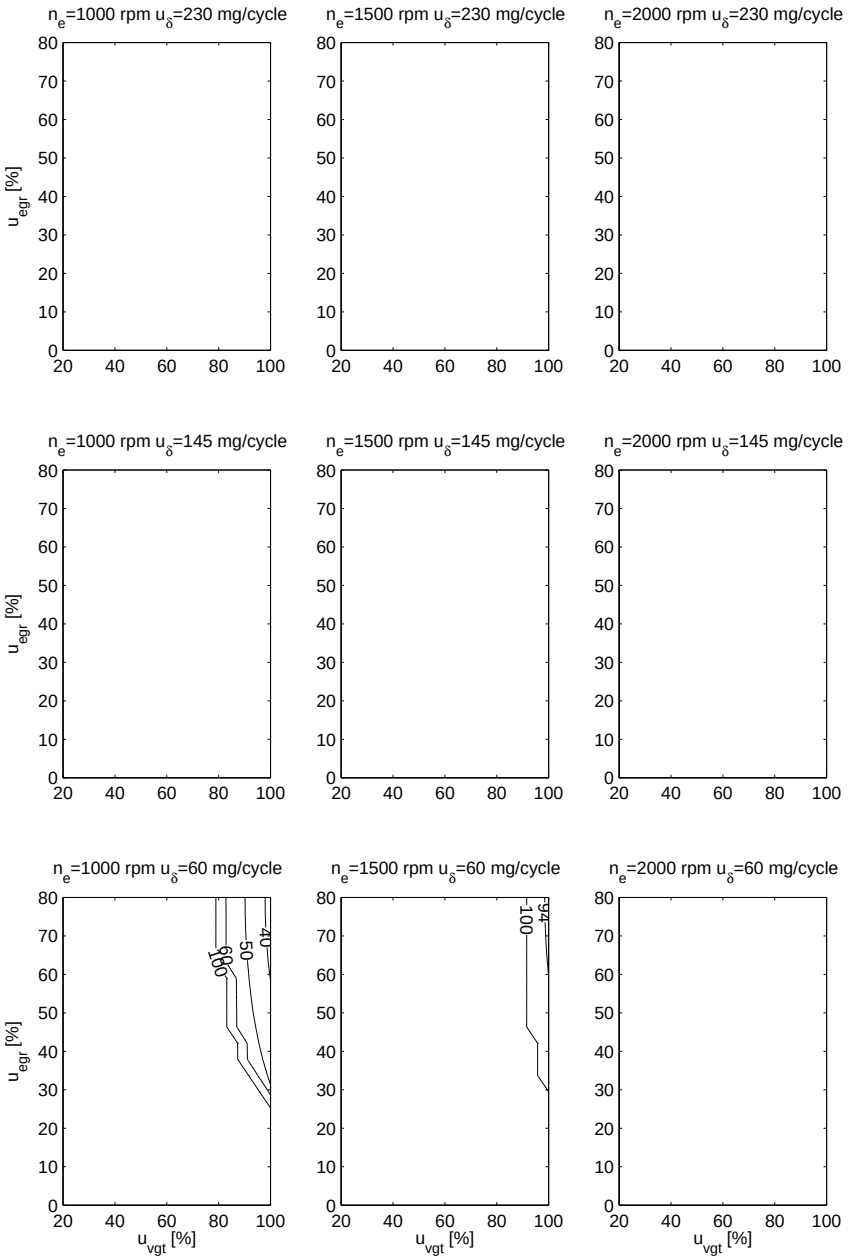

Figure 15: Contour plots of the relative undershoot, $x_N\,[\%]$, (see Eq. (2)) in a non-minimum phase behavior for the channel $u_{vgt} \rightarrow x_{egr}$ at 3 different n_e and 3 different u_δ.

Table 1: The minimum, mean, and maximum value of the response time τ in the entire operating region for the channels $u_{vgt} \to \lambda_O$, $u_{egr} \to \lambda_O$, $u_{vgt} \to x_{egr}$, and $u_{egr} \to x_{egr}$.

Channel	$u_{vgt} \to \lambda_O$	$u_{egr} \to \lambda_O$	$u_{vgt} \to x_{egr}$	$u_{egr} \to x_{egr}$
Minimum τ	0.10	0.12	0.07	0.16
Mean τ	1.10	0.97	0.20	0.17
Maximum τ	5.91	3.83	10.04	0.76

4.4 Operation pattern for the European Transient Cycle

A mapping of the operating points where the engine frequently operates is important in order to understand what system properties in the sections above that should be considered in the control design. This mapping is performed by simulating the complete control system in [5] during the European Transient Cycle. The control parameters are tuned using the method in [6] and the weighting factors $\gamma_{Me} = 1$ and $\gamma_{egr} = 1$. In Fig. 16, this simulation is plotted by first sampling the signals n_e, u_δ, u_{vgt}, and u_{egr} with a frequency of 10 Hz, and then dividing these simulated points into 9 different operating regions by selecting the nearest operating region to each simulated point. These operating regions correspond to the 9 different plots in Fig. 16 where each plot has u_{egr} on the y-axis and u_{vgt} on the x-axis, i.e. exactly as the contour plots in the previous sections. The percentage of simulated points in each operating region is also shown in the plots. Further, the lines where the sign reversals occur for the channels $u_{vgt} \to \lambda_O$, $u_{egr} \to \lambda_O$, and $u_{vgt} \to x_{egr}$ are shown in the plots.

Comparing Fig. 16 with Fig. 13 to 15, the conclusion is that the engine frequently operates in operating points where the sign reversal and the non-minimum phase occur for the channels $u_{vgt} \to \lambda_O$ and $u_{vgt} \to x_{egr}$, and that the engine does not frequently operate in operating points where the sign reversal and the non-minimum phase occur for $u_{egr} \to \lambda_O$. Consequently, it is important to consider the sign reversal and the non-minimum phase for $u_{vgt} \to \lambda_O$ and $u_{vgt} \to x_{egr}$ in a control design. The engine does not operate at $n_e > 1750$ rpm since the European Transient Cycle only consists of n_e that are lower than 1750 rpm.

4.5 Response time

The response time τ for the channels $u_{vgt} \to \lambda_O$, $u_{egr} \to \lambda_O$, $u_{vgt} \to x_{egr}$, and $u_{egr} \to x_{egr}$, respectively, are mapped over the entire operating region using the definition in Fig. 6. The result is presented in Appendix A, while the minimum, mean, and maximum value for each τ are shown in Tab. 1.

The variations of τ for the channels $u_{vgt} \to \lambda_O$, $u_{egr} \to \lambda_O$, and $u_{vgt} \to x_{egr}$ are larger compared to τ for the channel $u_{egr} \to x_{egr}$. This is because the channels $u_{vgt} \to \lambda_O$, $u_{egr} \to \lambda_O$, and $u_{vgt} \to x_{egr}$ have sign reversals. These three channels have small τ when the overshoot is large, which is in operating points with positive DC-gains near the sign reversals for $u_{vgt} \to \lambda_O$ and $u_{egr} \to \lambda_O$ and with negative DC-gains for $u_{vgt} \to x_{egr}$. The channels $u_{vgt} \to \lambda_O$, $u_{egr} \to \lambda_O$, and $u_{egr} \to x_{egr}$ have large τ in operating points with fully open EGR-valve, almost closed VGT, low n_e, and small u_δ. The channel $u_{vgt} \to x_{egr}$

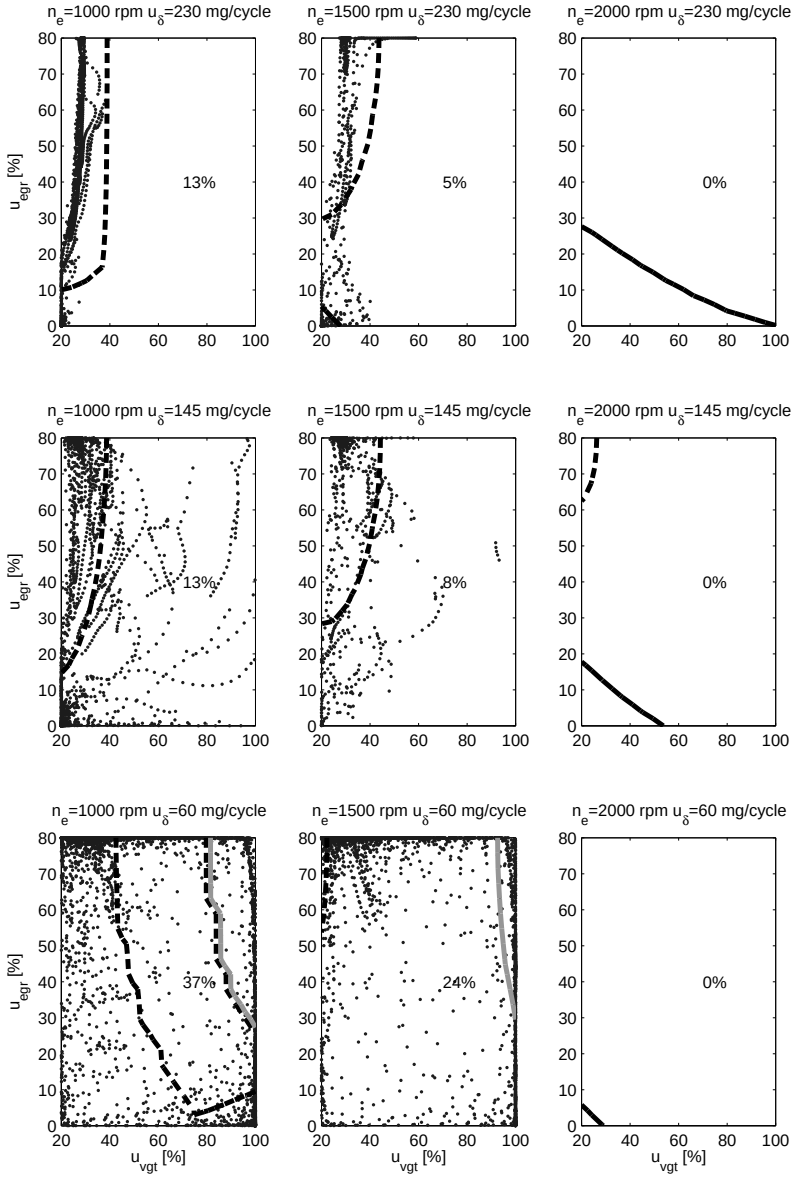

Figure 16: Operating points during European Transient Cycle simulations of a control system showing that the engine frequently operates in operating points where the sign reversal occurs for the channels $u_{vgt} \rightarrow \lambda_O$ (dashed black line) and $u_{vgt} \rightarrow x_{egr}$ (solid gray line), and that the engine does not frequently operate in operating points where the sign reversal occurs for the channel $u_{egr} \rightarrow \lambda_O$ (solid black line).

has a large τ in operating points with half to fully open EGR-valve, fully open VGT, medium n_e, and small u_δ.

5 Mapping of performance variables

Besides looking at dynamic responses of different loops, it is valuable to study the interaction. This is done in Sec. 5.1 for λ_O and x_{egr}. Further, in Sec. 5.2 the pumping losses are mapped to give insight into how to minimize the pumping losses.

5.1 System coupling in steady state

A mapping of the main performance variables λ_O and x_{egr} as function of u_{egr} and u_{vgt} in steady state is given in Fig. 17. The system is decoupled, in steady state, in one point if one of the contour lines is horizontal at the same time as the other line is vertical. This is almost the case in the gray areas in Fig. 17, see also the cross in the middle plot showing that the tangents to the contour lines are almost perpendicular in one point. The gray areas are near the sign reversals for $u_{vgt} \rightarrow \lambda_O$, $u_{egr} \rightarrow \lambda_O$, and $u_{vgt} \rightarrow x_{egr}$ since one of the contour lines is either horizontal or vertical at the sign reversals. In the operating regions that are not gray, the system is strongly coupled.

In the gray areas near the sign reversal for the channel $u_{vgt} \rightarrow \lambda_O$ (thick dashed line), u_{vgt} almost only affects x_{egr} and u_{egr} almost only affects λ_O. However, in the gray areas near the sign reversals for the channels $u_{egr} \rightarrow \lambda_O$ (thick solid line) and $u_{vgt} \rightarrow x_{egr}$ (dotted line) u_{egr} almost only affects x_{egr} and u_{vgt} almost only affects λ_O.

System coupling is also investigated in Appendix B by analyzing the relative gain array (RGA) showing that the system is strongly coupled. Input-output pairing for SISO controllers are also investigated showing that the best input-output pairing is $u_{egr} \rightarrow \lambda_O$ and $u_{vgt} \rightarrow x_{egr}$.

5.2 Pumping losses in steady state

A mapping of the pumping losses in steady state over the entire operating region gives insight into how to minimize the pumping work. Fig. 18 shows that the pumping losses $p_{em} - p_{im}$ decrease with increasing EGR-valve and VGT openings except at operating points with low torque, low engine speed, half to fully open EGR-valve, and half to fully open VGT, where there is a sign reversal in the gain from VGT to pumping losses. Further, the pumping losses are negative in operating points with half to fully open VGT, low to medium n_e, and medium to large u_δ, and the pumping losses are high in operating points with closed VGT and high n_e.

These observations are valuable since they give the basis for the development of a controller that besides control of the performance variables λ_O and x_{egr} also minimizes the pumping work. Further, the specific structure revealed in Fig. 18 makes it possible to employ a non-complicated control principle in an industrially adapted control structure, see [5].

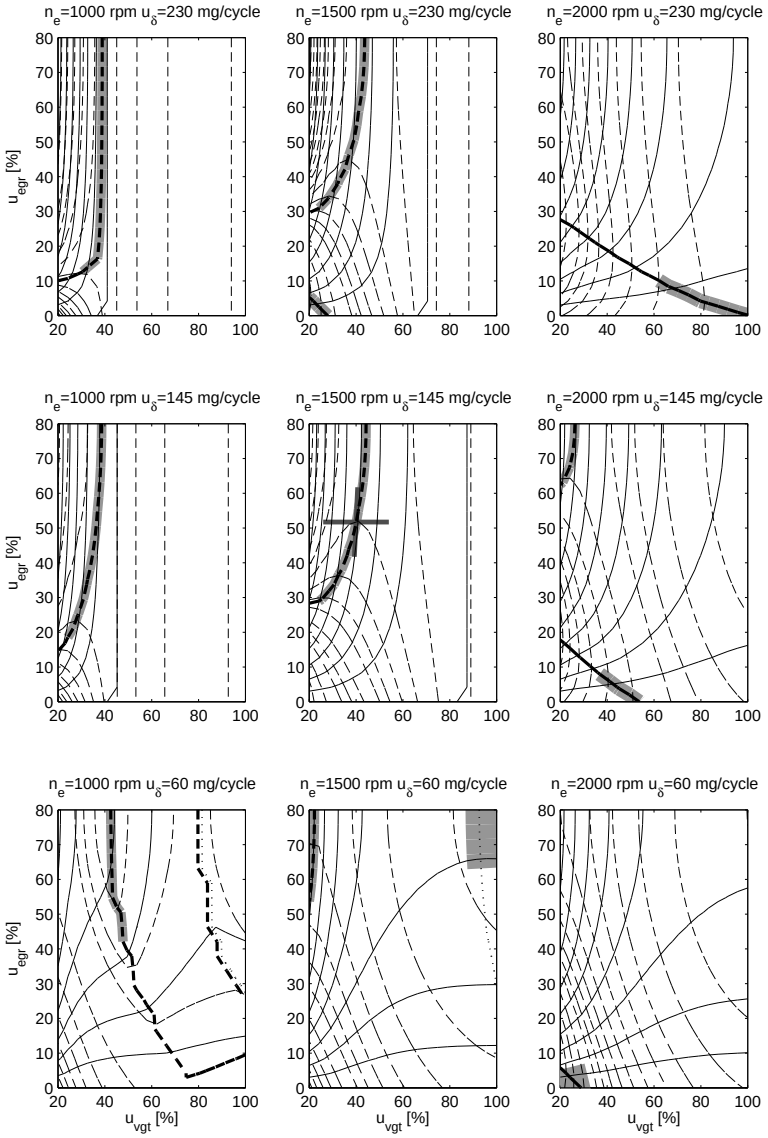

Figure 17: Contour plots of λ_O (thin dashed line) and x_{egr} (thin solid line) in steady-state at 3 different n_e and 3 different u_δ. The system from u_{egr} and u_{vgt} to λ_O and x_{egr} is strongly coupled in steady state in almost the entire operating region except for operating points in the gray areas. These areas are near the sign reversals for the channels $u_{vgt} \to \lambda_O$ (thick dashed line), $u_{egr} \to \lambda_O$ (thick solid line), and $u_{vgt} \to x_{egr}$ (dotted line). The cross in the middle plot shows an example of a point where the system is almost decoupled.

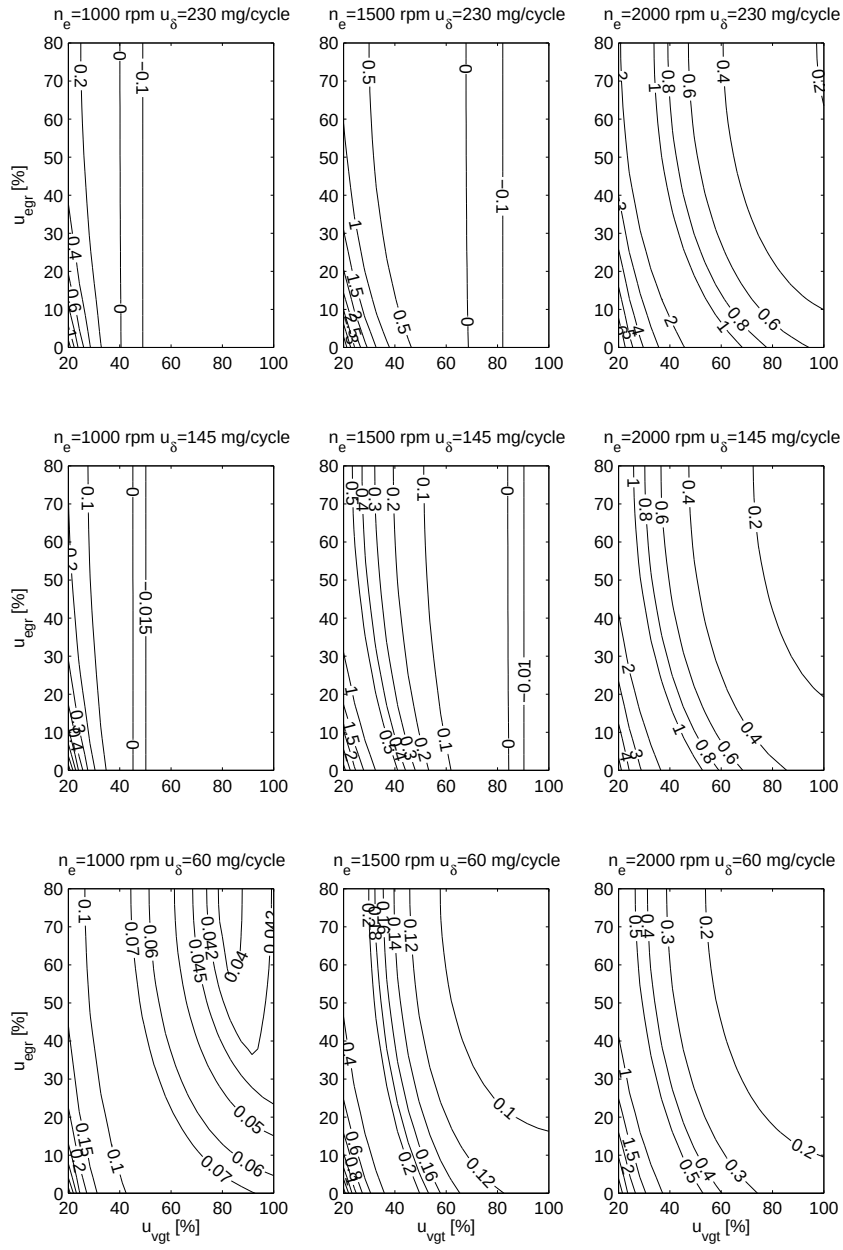

Figure 18: Contour plots of $p_{em} - p_{im}$ [bar] in steady-state at 3 different n_e and 3 different u_δ, showing that $p_{em} - p_{im}$ decreases with increasing EGR-valve and VGT opening, except in the left bottom plot where there is a sign reversal in the gain from u_{vgt} to $p_{em} - p_{im}$.

6 Conclusions

A system analysis of a diesel engine has been performed showing that the channels $u_{vgt} \rightarrow \lambda_O$, $u_{egr} \rightarrow \lambda_O$, and $u_{vgt} \rightarrow x_{egr}$ have non-minimum phase behaviors and sign reversals. The fundamental physical explanation of these system properties is that the system consists of two dynamic effects that interact: a fast pressure dynamics in the manifolds and a slow turbocharger dynamics. These two dynamic effects often work against each other which results in the system properties above. The analysis also shows that the engine frequently operates in operating points where these properties occur for the channels $u_{vgt} \rightarrow \lambda_O$ and $u_{vgt} \rightarrow x_{egr}$, and consequently, it is important to consider the sign reversal and the non-minimum phase behavior for these channels in a control design. Further, it was demonstrated that the four channels $(u_{vgt}, u_{egr}) \rightarrow (\lambda_O, x_{egr})$ have varying DC-gains and time constants. Furthermore, an analysis of linearized MIMO models of the engine shows that there is one zero in the right half plane over the complete operating region. Consequently, these MIMO models are non-minimum phase over the complete operating region. A mapping of the performance variables λ_O and x_{egr} and the relative gain array show that the system from u_{egr} and u_{vgt} to λ_O and x_{egr} is strongly coupled in a large operating region. It was also illustrated that the pumping losses $p_{em} - p_{im}$ decrease with increasing EGR-valve and VGT opening except for a small operating region (with low torque, low engine speed, half to fully open EGR-valve, and half to fully open VGT, where there is a sign reversal in the gain from VGT to pumping losses).

References

[1] J.B. Heywood. *Internal Combustion Engine Fundamentals.* McGraw-Hill Book Co, 1988.

[2] M. Jung. *Mean-Value Modelling and Robust Control of the Airpath of a Turbocharged Diesel Engine.* PhD thesis, University of Cambridge, 2003.

[3] I.V. Kolmanovsky, A.G. Stefanopoulou, P.E. Moraal, and M. van Nieuwstadt. Issues in modeling and control of intake flow in variable geometry turbocharged engines. In *Proceedings of* 18^{th} *IFIP Conference on System Modeling and Optimization*, Detroit, July 1997.

[4] C. Vigild. *The Internal Combustion Engine Modelling, Estimation and Control Issues.* PhD thesis, Technical University of Denmark, Lyngby, 2001.

[5] Johan Wahlström. Control of EGR and VGT for emission control and pumping work minimization in diesel engines. Technical report, Linköping University, 2006.

[6] Johan Wahlström, Lars Eriksson, and Lars Nielsen. Controller tuning based on transient selection and optimization for a diesel engine with EGR and VGT. In *Electronic Engine Controls*, number 2008-01-0985 in SAE Technical paper series SP-2159, SAE World Congress, Detroit, USA, 2008.

[7] Johan Wahlström and Lars Eriksson. Modeling of a diesel engine with VGT and EGR capturing sign reversal and non-minimum phase behaviors. Technical report, Linköping University, 2009.

A Response time

The response time τ (see Fig. 6) for the channels $u_{vgt} \rightarrow \lambda_O$, $u_{egr} \rightarrow \lambda_O$, $u_{vgt} \rightarrow x_{egr}$, and $u_{egr} \rightarrow x_{egr}$ are shown in Fig. 19 to 22 over a large operating region.

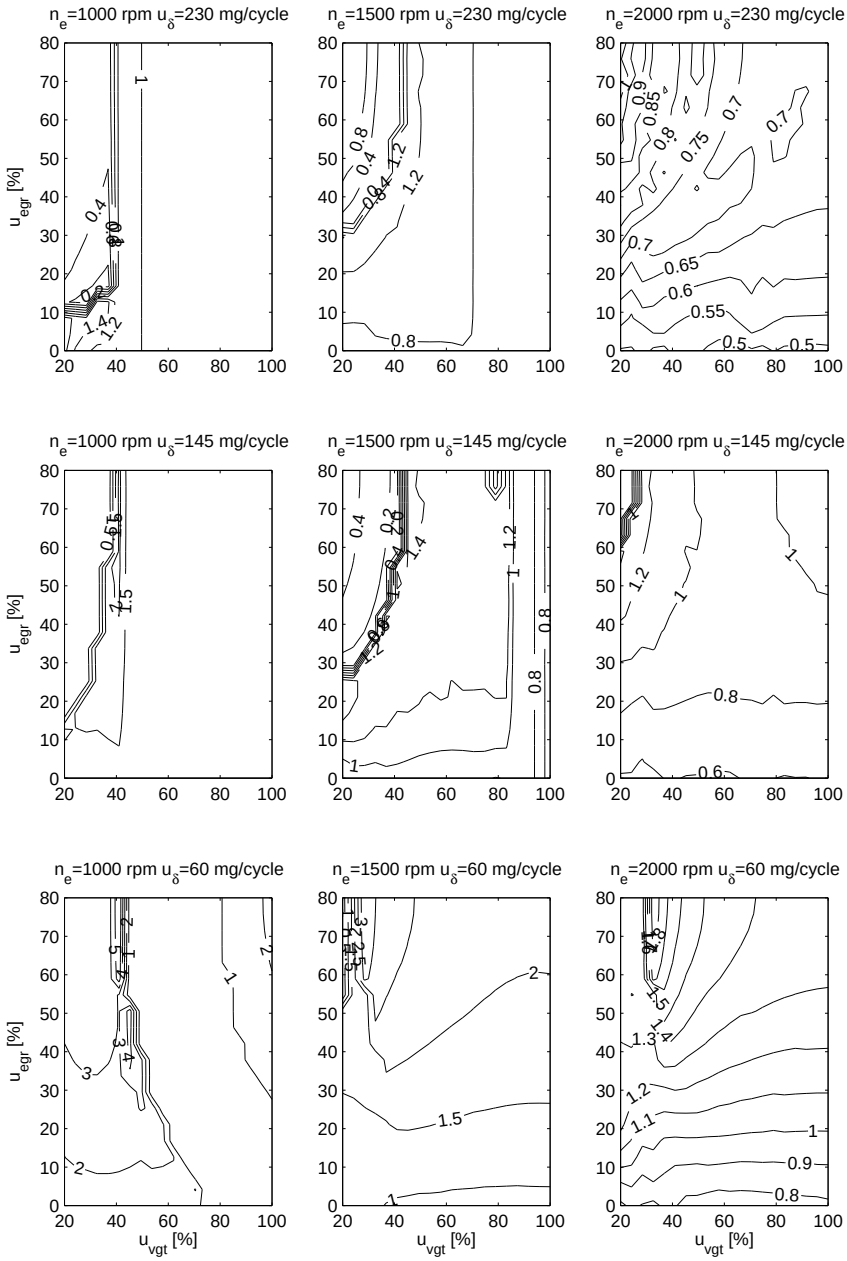

Figure 19: Contour plots of the response time, τ [s], for the channel $u_{vgt} \rightarrow \lambda_O$ at 3 different n_e and 3 different u_δ, i.e. 3*3=9 different n_e and u_δ points.

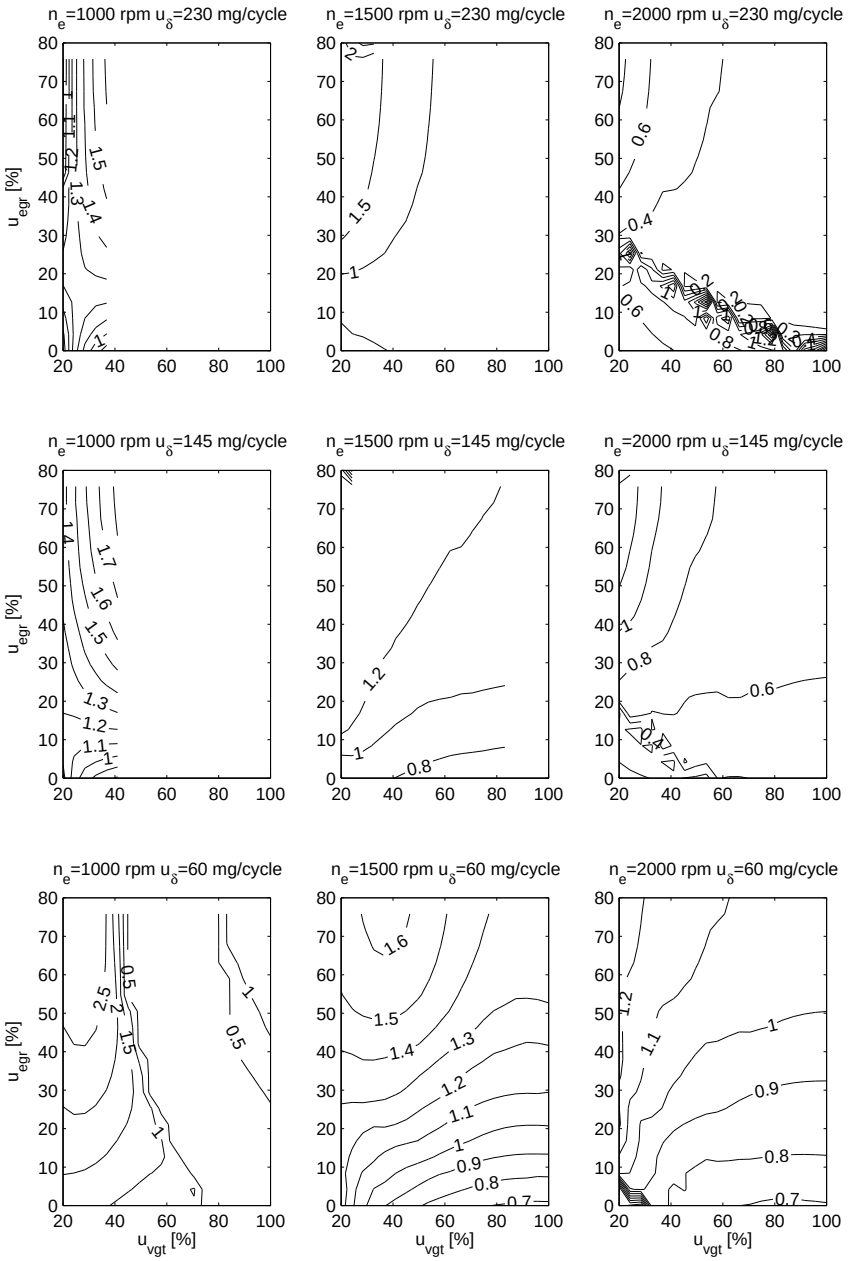

Figure 20: Contour plots of the response time, τ [s], for the channel $u_{egr} \rightarrow \lambda_O$ at 3 different n_e and 3 different u_δ, i.e. 3*3=9 different n_e and u_δ points.

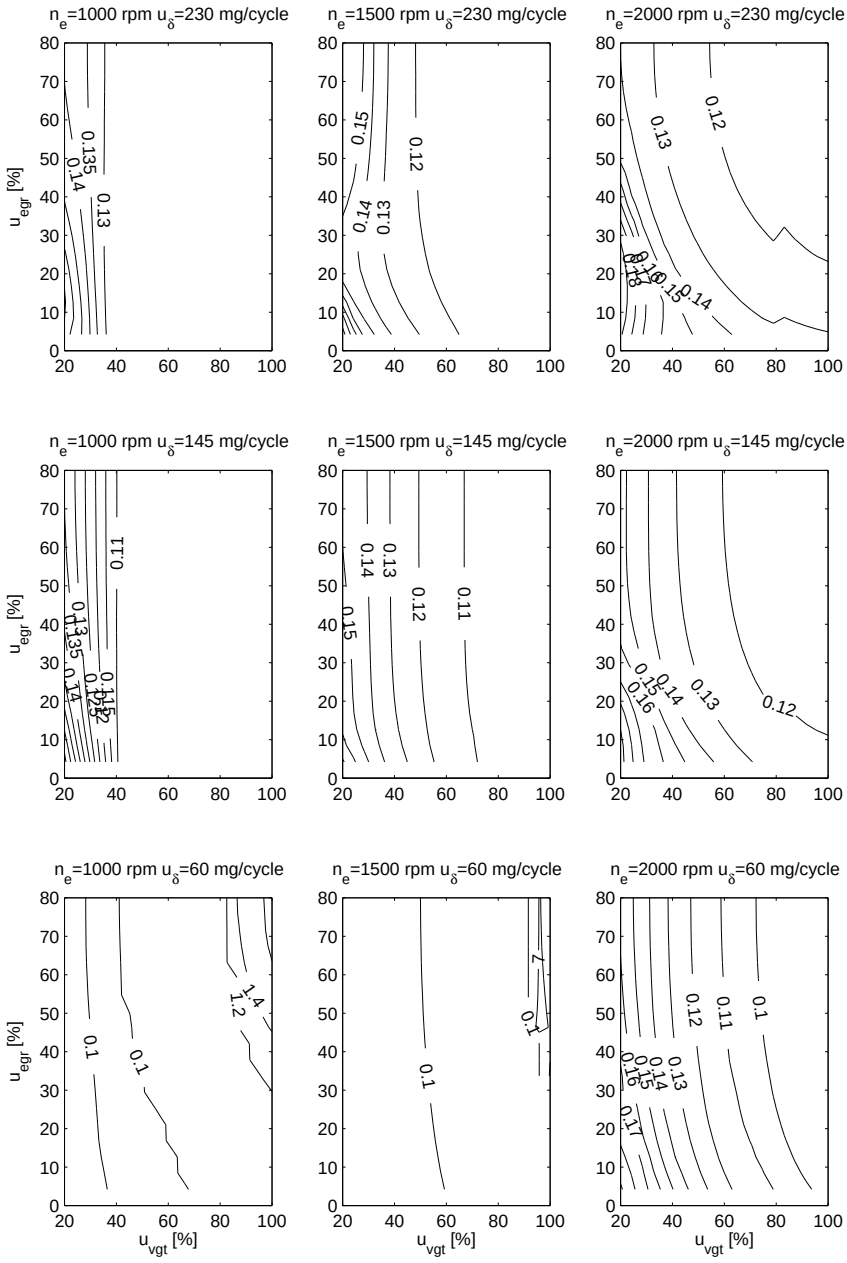

Figure 21: Contour plots of the response time, τ [s], for the channel $u_{vgt} \rightarrow x_{egr}$ at 3 different n_e and 3 different u_δ, i.e. 3*3=9 different n_e and u_δ points.

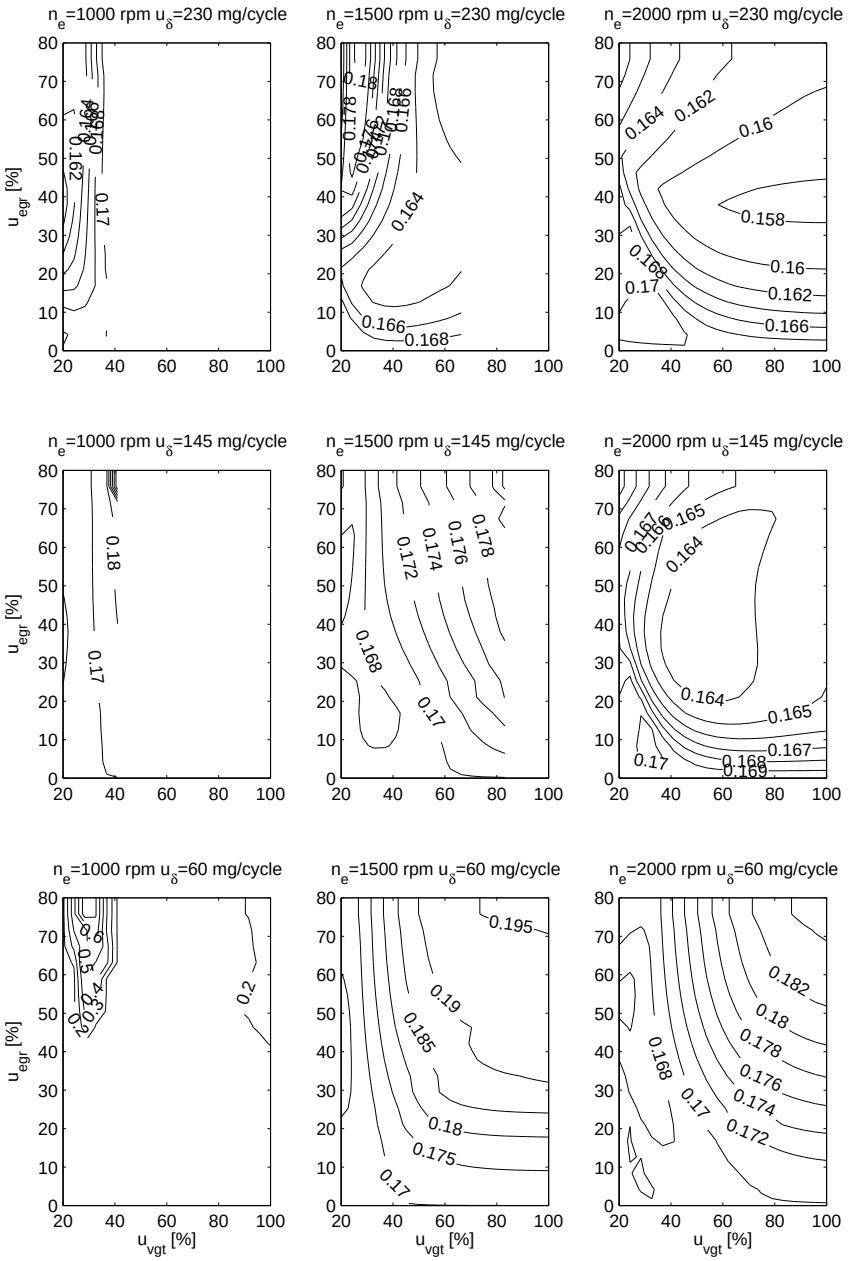

Figure 22: Contour plots of the response time, τ [s], for the channel $u_{egr} \rightarrow x_{egr}$ at 3 different n_e and 3 different u_δ, i.e. 3*3=9 different n_e and u_δ points.

B Relative gain array

Mappings of the relative gain array (RGA) for linearized MIMO models of the engine over the entire operating region are performed in order investigate system coupling and input-output pairing for SISO controllers. For a matrix G, RGA is defined as

$$RGA(G) = G. * (G^{\dagger})^T \tag{6}$$

where ".$*$" is the element-by-element multiplication and the pseudo inverse is defined as

$$G^{\dagger} = (G^* G)^{-1} G^* \tag{7}$$

where G^* is the conjugate transpose of the matrix G.

RGA is analyzed for the linearized models (4) in Sec. 4.2, giving the following transfer functions

$$G_i(s) = C_i(s\,I - A_i)^{-1} B_i \tag{8}$$

for each operating point i and the following relation between inputs and outputs

$$\begin{pmatrix} \lambda_O \\ x_{egr} \end{pmatrix} = G_i(s) \cdot \begin{pmatrix} u_{egr} \\ u_{vgt} \end{pmatrix} \tag{9}$$

When investigating the best input-output pairing for SISO controllers, there are two main rules to follow:

1. Choose input-output pairings where the corresponding elements in the matrix $RGA(G_i(j\omega_c))$ are close to 1 in the complex plane. Here, ω_c is the desired bandwidth of the closed-loop system.

2. Avoid input-output pairings where the corresponding elements in the matrix $RGA(G_i(0))$ are negative.

In order to follow rule 1 above, RGA is mapped in the following way. For

$$RGA(G_i(j\omega_c)) = \begin{pmatrix} g_{11} & g_{12} \\ g_{21} & g_{22} \end{pmatrix} \tag{10}$$

with $\omega_c = 1/4$ rad/s

$$s_1 = |g_{11} - 1| + |g_{22} - 1| \tag{11}$$

$$s_2 = |g_{21} - 1| + |g_{12} - 1| \tag{12}$$

are calculated. If s_1 or s_2 are small, the corresponding elements in (10) are close to 1. The variables s_1 and s_2 are mapped in Fig. 23 and 24 respectively showing that each of these variables are smaller than 1 in the gray areas. The points where the engine operates during the European Transient Cycle are also mapped in the figures in the same way as in Fig. 16. Consequently, the goal is to choose an input-output pairing so that the engine frequently operates in the gray areas. It can be seen that the engine operates outside the gray areas in both Fig. 23 and 24 for some operating points. Consequently, the system is strongly coupled in these points. For $u_\delta \geq 145$ mg/cycle the engine operates more frequently in the gray areas in Fig. 23 than in Fig. 24. However, for $u_\delta = 60$ mg/cycle it is the reversed relation, i.e. the engine operates more frequently in the gray areas in Fig. 24 than in Fig. 23. On the other hand, one of the control inputs are

often saturated when $u_\delta = 60$ mg/cycle and when this occur, there is no pairing problem. Consequently, according to rule 1 the best input-output pairing is

$$u_{egr} \rightarrow \lambda_O$$
$$u_{vgt} \rightarrow x_{egr}$$

In order to follow rule 2 above, RGA is mapped in the following way. For

$$RGA(G_i(0)) = \begin{pmatrix} h_{11} & h_{12} \\ h_{21} & h_{22} \end{pmatrix} \tag{13}$$

the variables h_{11} and h_{21} are mapped in Fig. 25 and 26 respectively showing that each of these variables are greater or equal to zero in the gray areas. The variable h_{12} is greater or equal to zero in the same area as h_{21} and h_{22} is greater or equal to zero in the same area as h_{11}. In the same way as in Fig. 23 and 24 the goal is to choose an input-output pairing so that the engine frequently operates in the gray areas. The result is that the engine operates more frequently in the gray areas in Fig. 25 than in Fig. 26. It is only a small white area in the left bottom plot in Fig. 25 where $h_{11} < 0$ and where the engine operates for some few operating points. Consequently, even for rule 2 the best input-output pairing is

$$u_{egr} \rightarrow \lambda_O$$
$$u_{vgt} \rightarrow x_{egr}$$

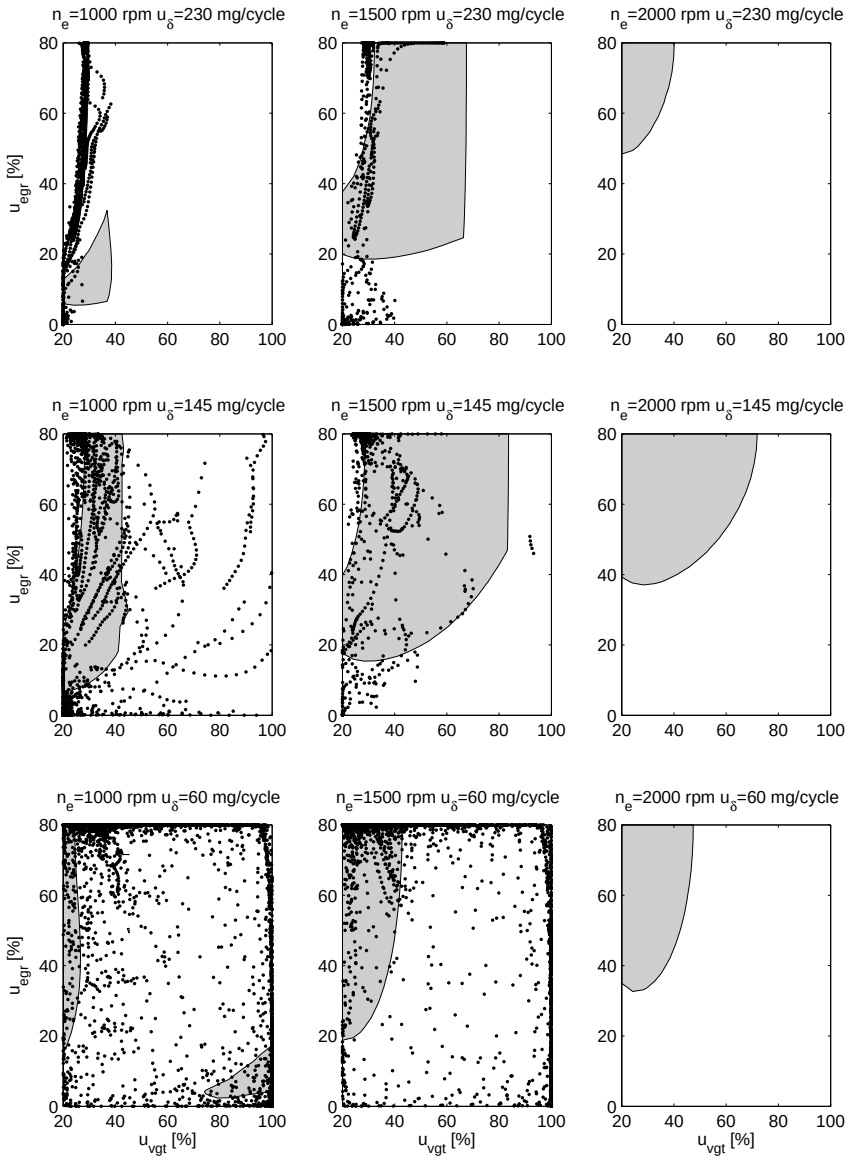

Figure 23: A mapping of s_1, defined by (11), showing that $s_1 < 1$ in the gray areas. The points where the engine operates during the European Transient Cycle are also mapped showing that for $u_\delta \geq 145$ mg/cycle the engine operates more frequently in the gray areas than in Fig. 24.

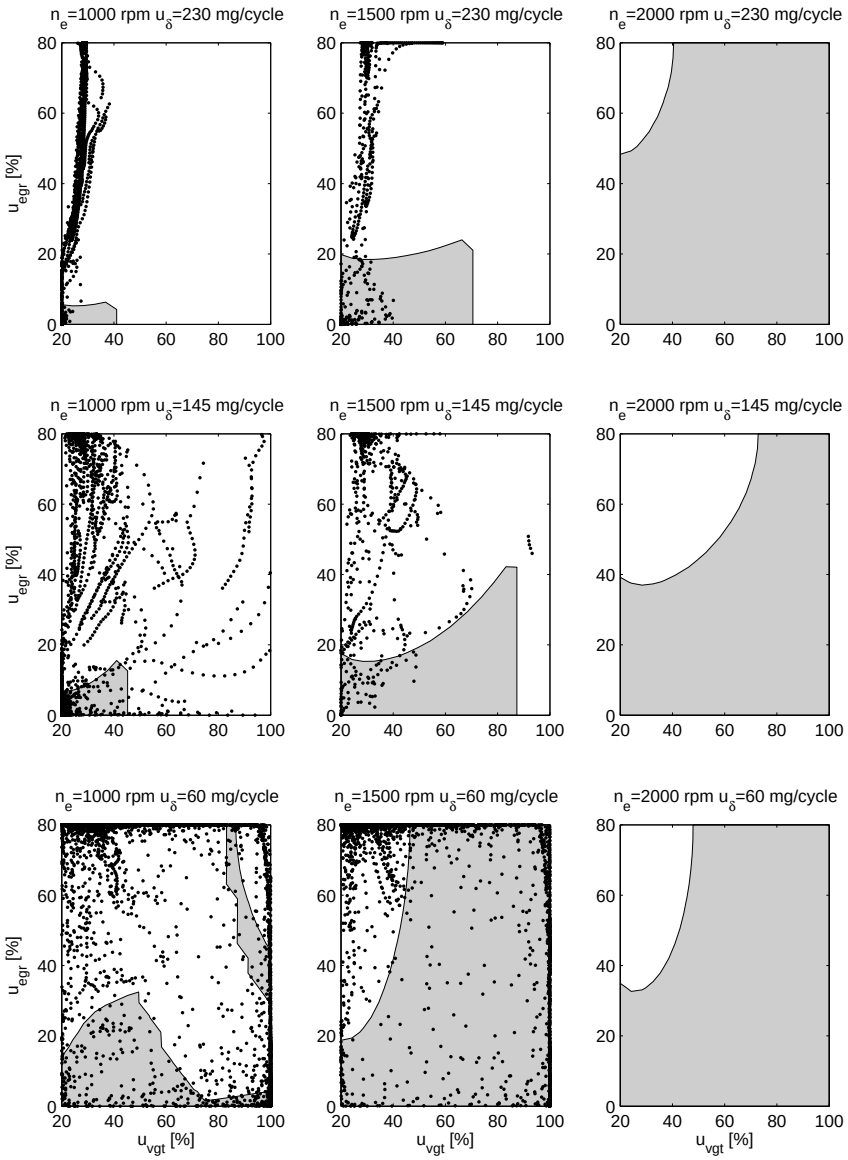

Figure 24: A mapping of s_2, defined by (12), showing that $s_2 < 1$ in the gray areas. The points where the engine operates during the European Transient Cycle are also mapped.

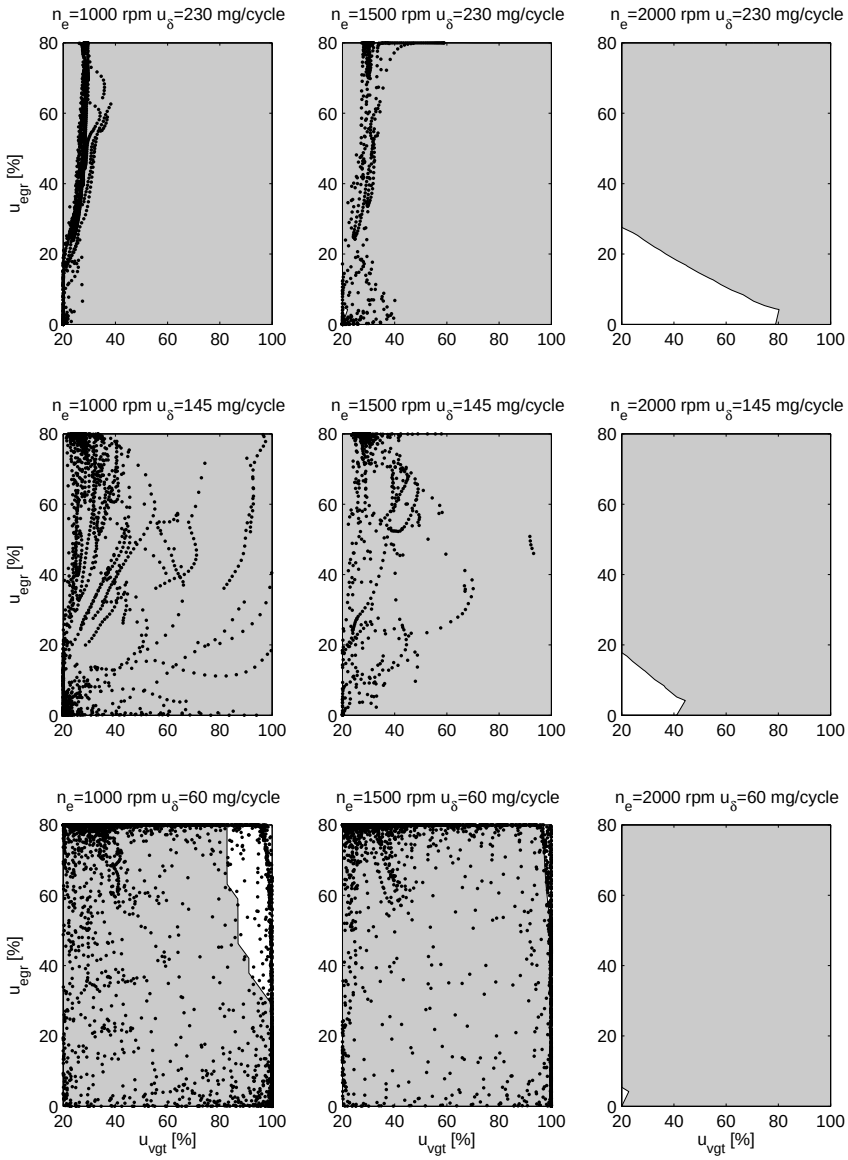

Figure 25: A mapping of h_{11}, defined by (13), showing that $h_{11} \geq 0$ in the gray areas. The points where the engine operates during the European Transient Cycle are also mapped showing that the engine operates more frequently in the gray areas than in Fig. 26.

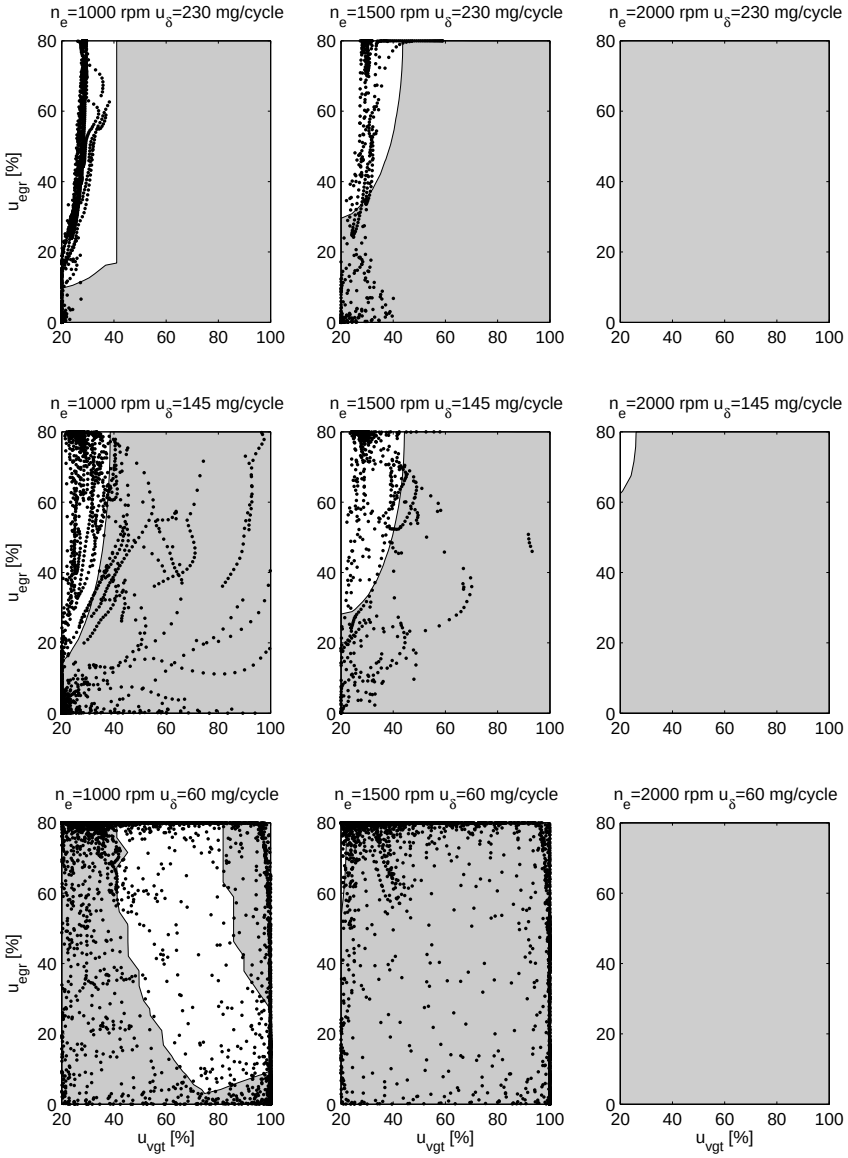

Figure 26: A mapping of h_{21}, defined by (13), showing that $h_{21} \geq 0$ in the gray areas. The points where the engine operates during the European Transient Cycle are also mapped.